https://doi.org/10.5194/acp-2019-788
Preprint. Discussion started: 16 December 2019


Atmospheric Chemistry and Physics Discussions

# Parameterized reactivity of hydroxy radical, ozone, nitrate radical and atmospheric oxidation capacity during summer at a suburban site between Beijing and Tianjin

Yuan Yang[1,2], Yonghong Wang[3], Dan Yao[1,2,6], Dongsheng Ji[1], Jie Sun[1], Yinghong Wang[1], Shuman Zhao[1,2], Wei Huang[1,2], Shuanghong Yang[1,5], Wenkang Gao[1], Zirui Liu[1], Bo Hu[1], Renjian Zhang[1], Limin Zeng[4], Tuukka Petäjä[3], Veli-Matti Kerminen[3], Markku Kulmala[3], Yuesi Wang[1,2,6]

[1] Institute of Atmospheric Physics, Chinese Academy of Sciences, Beijing 100029, China

[2] University of the Chinese Academy of Sciences, Beijing 100049, China

[3] Institute for Atmospheric and Earth System Research / Physics, Faculty of Science, P.O.Box 64, 00014 University of Helsinki, Helsinki, Finland

[4] State Joint Key Laboratory of Environmental Simulation and Pollution Control, College of Environmental Sciences and Engineering, Peking University, Beijing 100871, China

[5] Department of Environmental Science and Engineering, Beijing University of Chemical Technology, Beijing 10029, China

[6] Center for Excellence in Regional Atmospheric Environment, Institute of Urban Environment, Chinese Academy of Sciences, Xiamen 361021, China

Submitted to： Atmospheric Chemistry and Physics

Corresponding to: Yonghong Wang, yonghong.wang@helsinki.fi;

Yuesi Wang, wys@mail.iap.ac.cn

:

https://doi.org/10.5194/acp-2019-788
Preprint. Discussion started: 16 December 2019


Atmospheric Chemistry and Physics Discussions

**Abstract**

Hydroxyl (OH) radicals, nitrate ($NO_3$) radicals, and ozone ($O_3$) play central roles in the troposphere because they control the lifetimes of many trace gases that resulted from anthropogenic and biogenic origins. To estimate the self-cleaning capacity of the atmosphere, the reactivities of OH, $NO_3$ and $O_3$ were comprehensively analyzed based on a parameterization method at a suburban site in Xianghe in the North China Plain from 6 July 2018 to 6 August 2018. The site had suffered the most abundant annual mean VOCs concentrations according to a network observation from 2012-2014 (personal communication). The total OH reactivity, $R_{OH}^{\text{total}}$, $NO_3$ reactivity, $R_{NO_3}^{\text{total}}$, and $O_3$ reactivity, $R_{O_3}^{\text{total}}$, at the site varied from 8.5 $s^{-1}$ to 68.1 $s^{-1}$, 0.7 $s^{-1}$ to 27.5 $s^{-1}$, and $3.3\times10^{-4}$ $s^{-1}$ to $1.8\times10^{-2}$ $s^{-1}$ with campaign-averaged values of 25.6±9.7 $s^{-1}$, 2.2±2.6 $s^{-1}$ and 1.2±1.7×$10^{-3}$ $s^{-1}$ (± standard deviation), respectively. $NO_x$ ($NO+NO_2$) were by far the main contributors to the $R_{OH}^{\text{total}}$, $R_{NO_3}^{\text{total}}$ and $R_{O_3}^{\text{total}}$, with average values of 47, 99 and 99%, respectively. Isoprene dominated the OH and $NO_3$ reactivity towards TVOCs ($R_{OH}^{\text{TVOCs}}$ and $R_{NO_3}^{\text{TVOCs}}$), accounting for 40% and 77%, respectively. However, alkenes dominated the $O_3$ reactivity towards TVOCs ($R_{O_3}^{\text{TVOCs}}$), representing 66% of $R_{O_3}^{\text{total}}$. $R_{OH}^{\text{total}}$, $R_{NO_3}^{\text{total}}$ and $R_{O_3}^{\text{total}}$ displayed a similar diurnal variation with the lowest during the afternoon and the highest during rush hours, and the diurnal profile of $NO_x$ appears to be the major driver for the diurnal profiles of $R_{OH}^{\text{total}}$, $R_{NO_3}^{\text{total}}$ and $R_{O_3}^{\text{total}}$. The calculated atmospheric oxidative capacity (AOC) was up to $4.4\times10^{8}$ molecules $cm^{-3}$ $s^{-1}$ with campaign-averaged values of $3.1\times10^{7}$ molecules $cm^{-3}$ $s^{-1}$ dominated by OH radicals ($2.9\times10^{7}$ molecule $cm^{-3}$ $s^{-1}$, 95%), $O_3$ ($1.2\times10^{6}$ molecule $cm^{-3}$ $s^{-1}$, 4%) and $NO_3$ radicals ($1.7\times10^{5}$ molecule $cm^{-3}$ $s^{-1}$, 1%). The reaction with OH radicals was the dominant volatile organic compounds (VOCs) loss except for trans-2-butene, cis-2-butene, trans-2-pentene, propylene, 1-butene, 1-pentene, 1-hexene, acetone and styrene, where the reaction with $O_3$ was more important for their loss rates. Compared with anthropogenic hydrocarbons, the oxidation by the $NO_3$ radical was more important for the nighttime integral of isoprene loss rates. Overall, the present study may provide some useful suggestions for VOC pollution control in the Xianghe and North China Plain. To better understanding the trace gas reactivity and AOC, further studies, especially direct observations of the OH and $NO_3$ radical concentrations and their reactivities, are required.

**Keywords:** VOCs; radical reactivity; atmospheric oxidation capacity; loss rate; North China Plain

https://doi.org/10.5194/acp-2019-788
Preprint. Discussion started: 16 December 2019


Atmospheric Chemistry and Physics Discussions

## 1 Introduction

In the planetary boundary layer, overwhelming quantities of trace gases from both biogenic and anthropogenic origins (Guenther et al., 1995;Piccot et al., 1992;Chen et al., 2019;Li et al., 2019b;Wang et al., 2019b) are also a major part transformed by reactions with free radicals such as hydroxyl (OH) radicals, nitrate ($NO_3$) radicals, and ozone ($O_3$) on local to global scales (Atkinson and Arey, 2003;Heard and Pilling, 2003), with the dominant reaction depending on the time of day and specific trace gases. Ultimately, these processes lead to the formation of a series of important secondary pollutants, including tropospheric $O_3$ and secondary organic aerosol (SOA) (Goldstein and Galbally, 2007).

OH radicals control the daytime oxidation capacity of the atmosphere (Heard and Pilling, 2003), initiating and participating in many oxidation reaction processes. OH exhibits a high reactivity to many atmospheric trace gases, such as carbon monoxide (CO), nitrogen oxides ($NO_x$=NO+$NO_2$) and volatile organic compounds (VOCs) (Kovacs et al., 2003;Sadanaga et al., 2005). The total OH reactivity ($R_{OH}$) is the sum of the products of the concentrations and respective reaction rate coefficients for all gases that react with OH. The total OH reactivity is equivalent to the inverse of the lifetime of OH ($s^{-1}$) in the presence of those atmospheric constituents. $R_{OH}$ can be measured directly ($R_{OH}^{\mathrm{measured}}$), modeled ($R_{OH}^{\mathrm{modeled}}$) or calculated from individual trace gas measurements ($R_{OH}^{\mathrm{calculated}}$). The online techniques used to determine $R_{OH}^{\mathrm{measured}}$ include the flow tube with sliding injector method, a comparative rate method and a laser flash photolysis pump probe technique (Yang et al., 2016;Whalley et al., 2016;Lou et al., 2010). Based on these online methods, the values of $R_{OH}$ have been measured in urban, suburban, remote and forest areas during the last decade. The urban areas investigated included Nashville, USA (SOS) (Kovacs et al., 2003), New York, USA (PMTACS-NY2004) (Ren et al., 2006a), Mexico City, Mexico (MCMA-2003) (Shirley et al., 2006), Houston, USA (TRAMP2006) (Mao et al., 2010), Paris, France (MEGAPOLI) (Dolgorouky et al., 2012), London, UK (ClearfLo) (Whalley et al., 2016)and Beijing, China (Yang et al., 2017). The ranges of $R_{OH}^{\mathrm{measured}}$ in these urban areas ranged from 1 $s^{-1}$ in clean air to 200 $s^{-1}$ in extremely polluted air in the atmospheric boundary layer, and $NO_x$, CO, formaldehyde and VOCs were the main contributors (Ferracci et al., 2018). The suburban areas investigated included Whiteface Mountain, USA (PMTACS-NY2002) (Ren et al., 2006b), Weybourne, UK (TORCH-2) (Lee et al.,

https://doi.org/10.5194/acp-2019-788
Preprint. Discussion started: 16 December 2019


Atmospheric Chemistry and Physics Discussions

2010), Yufa, China (CAREBeijing-2006) (Lu et al., 2010), Backgarden, China (PRIDE-PRD) (Lou et al., 2010), Jülich, Germany (HOx Comp) (Elshorbany et al., 2012), Ersa, Corsica (CARBOSOR-ChArMeX) (Zannoni et al., 2017) and Heshan, China (Yang et al., 2017). The ranges of $R_{OH}^{\text{measured}}$ in these suburban areas ranged from 4.6 to 31.4 $s^{-1}$. $R_{OH}^{\text{modeled}}$ was modeled using zero-dimensional box model based on the Regional Atmospheric Chemical Mechanism to compare them with the measurements or calculations (Lou et al., 2010;Whalley et al., 2016;Ferracci et al., 2018;Yang et al., 2017). $R_{OH}^{\text{calculated}}$ is the sum of the OH reactivities that are attributed to measured trace gases, which is used extensively as a matrix to estimate the initial peroxyl radical ($RO_2$) formation rate under optimum reaction conditions (Carter, 2012;Liu et al., 2008;Warneke, 2004). This matric does not account for chain termination or propagation steps, nor does it properly capture differences in VOC production of $RO_2$ during photolysis or reaction with other oxidants; however, this matric does provide at least some useful approximation of the relative contribution of individual VOCs to daytime photochemistry (Goldan et al., 2004;Benedict et al., 2019). The concentrations (in molecules $cm^{-3}$) of trace gases and the reaction rate constants ($k_{\text{trace gase+OH}}$ in $cm^3$ $molecule^{-1}$ $s^{-1}$) of the respective trace gases with the OH radical are the key factors for computing $R_{OH}^{\text{calculated}}$. In general, the trace gases have been considered when calculating $R_{OH}^{\text{calculated}}$ include VOCs, CO, $NO_x$ and $SO_2$. Reportedly, the contribution from the $NO_x$ exceeds 50% for the cities of Paris, Tokyo, New York and Beijing, showing the large influence of traffic-related emissions on the $R_{OH}^{\text{calculated}}$ (Dolgorouky et al., 2012;Ren, 2003;Yang et al., 2017;Yoshino et al., 2006), but the contribution from the VOCs reaches 50% in Mexico and Houston (Mao et al., 2010;Shirley et al., 2006).

As OH levels are vastly reduced during nighttime due to missing photolysis, the $NO_3$ formed by the slow reaction of $NO_2 + O_3 \rightarrow NO_3 + O_2$ is the main initiator of nighttime oxidation chemistry in the troposphere due to the lack of photolysis and its elevated mixing ratios at night (Asaf et al., 2009;Geyer et al., 2001). $NO_3$ reacts significantly with unsaturated VOCs such as isoprene, certain alkenes and aromatics via additions to a >C=C< double bond, which can initiate the formation of peroxyl radicals ($HO_2$ and $RO_2$) and even of OH (Geyer et al., 2001). The high $NO_3$ mixing ratios and the large reaction rate constants with several unsaturated VOCs result in $NO_3$ being the dominant sink of many unsaturated VOCs during nighttime. The role of $NO_3$ as an oxidizing agent may be assessed via its total reactivity $R_{NO_3}$ towards trace gases (or inverse lifetime $s^{-1}$). $R_{NO_3}$ is

https://doi.org/10.5194/acp-2019-788
Preprint. Discussion started: 16 December 2019


Atmospheric Chemistry and Physics Discussions

an indication of nighttime oxidation rates of trace gases with direct impacts on $NO_x$ levels and indirect impacts on heterogeneous $NO_x$ losses and $ClNO_2$ formation (Liebmann et al., 2017). As frequently reported for $R_{OH}$, $R_{NO_3}$ can be measured online ($R_{NO_3}^{\text{measured}}$) or calculated from summing loss rates for a set of reactive trace gases ($R_{NO_3}^{\text{calculated}}$). Previous work on $R_{NO_3}^{\text{measured}}$ has revealed a strong diel variation. For instance, the $R_{NO_3}^{\text{measured}}$ obtained during the IBAIRN campaign, which was carried out in the boreal forest of Finland, Hyytiälä, displayed a strong diel variation with a campaign-averaged nighttime mean value of 0.11 $s^{-1}$ compared to a daytime value of 0.04 $s^{-1}$ (Liebmann et al., 2018a), but varied from 0.005 to 0.1 $s^{-1}$ during nighttime and reached values as high as 1.4 $s^{-1}$ in the daytime during NOTOMO (Liebmann et al., 2017).

Along with reactions with the OH and $NO_3$ radicals, trace gases are oxidized in the troposphere by reactions with $O_3$. Although $O_3$ reacts significantly with alkenes, for most VOCs, the reaction rate of $O_3$ is much slower than the reaction rate of OH and $NO_3$. However, $O_3$ is very important because it is present at elevated mixing ratios in clean or contaminated atmospheres (Wang et al., 2013). The rate constants for some reactions of $O_3$ with alkenes are even comparable to those with $NO_3$ (Atkinson and Arey, 2003). The total reaction frequency of $O_3$ with trace gases ($R_{O_3}$) can reflect the role of $O_3$ as an oxidizing agent. Direct measurements of $R_{O_3}$ were not available until very recently (Geyer, 2003); hence, the reactivity of $O_3$ has traditionally been calculated ($R_{O_3}^{\text{calculated}}$) by summing the reactivities due to individual reactive trace gases. $R_{O_3}^{\text{calculated}}$ obtained during the BERLIOZ campaign revealed that terpenes (20%), isoprene (20%), and other alkenes (60%) were the dominant contributors during the night of 20 and 21 July but arose mainly (83%) from non-biogenic alkene during the night of 4 and 5 August (Geyer, 2003).

As mentioned above, OH radical, $NO_3$ radical, and $O_3$-initiated reactions of trace gases with different mechanisms result in different rate coefficients and thus different reactivities. Recently, a few studies on $R_{OH}^{\text{measured}}$, $R_{OH}^{\text{modeled}}$ or $R_{OH}^{\text{calculated}}$ have been conducted in China (Lou et al., 2010;Fuchs et al., 2017b;Yang et al., 2017;Lu et al., 2010;Williams et al., 2016;Lyu et al., 2019). However, comprehensive evaluations of $R_{OH}^{\text{calculated}}$, $R_{NO_3}^{\text{calculated}}$ and $R_{O_3}^{\text{calculated}}$ are scarce. In this study, $R_{OH}^{\text{calculated}}$, $R_{NO_3}^{\text{calculated}}$ and $R_{O_3}^{\text{calculated}}$ were conducted at a suburban site (Xianghe) in the North China Plain during an intensive measurement campaign in the summer of 2018. By

https://doi.org/10.5194/acp-2019-788
Preprint. Discussion started: 16 December 2019


Atmospheric Chemistry and Physics Discussions

combining OH and $NO_3$ concentrations determined using parameterization methods, the oxidation capacities of OH, $NO_3$ and $O_3$ were compared to estimate their contributions to the atmospheric oxidation capacity.

## 2 Methodology

### 2.1 Site description

The sampling site is located at the Xianghe Atmospheric Observatory (39.798 °N, 116.958 °E; 15 m above sea level), which is operated by the Institute of Atmospheric Physics (IAP)/Chinese Academy of Sciences (CAS). The sampling site is a typical suburban site in the seriously polluted Beijing-Tianjin-Hebei large urban region, which is approximately 50 km southeast of Beijing, 75 km northwest of Tianjin, and 35 km northeast of Langfang in the Hebei Province. The sampling site is approximately 4 km west of the downtown center and is surrounded by residential areas and agricultural land (see Figure 1).

### 2.2 Experimental method

**Criteria pollutants** $O_3$ was measured using a UV photometric $O_3$ analyzer (Model 49C/I, Thermo-Fisher Scientific, United States) with the lowest detection limit of 2.0 ppb, precision of ±1.0 ppb, zero drift of less than 1.0 ppb $(24\ h)^{-1}$, span drift of less than 1% full scale per month, and response time of 10 s. $NO_x$ was measured using a chemiluminescence $NO_x$ Analyzer (Model 42C/I) with the lowest detection limit of 0.4 ppb, precision of ±0.4 ppb, zero drift of less than 0.4 ppb $(24\ h)^{-1}$, span drift of less than 1% per 24 h, and response time of 40 s. $NO_y$ was measured using a chemiluminescence NO-DIF-NOy Analyzer (Model 42C/I) with the lowest detection limit of 50 ppt, span drift of less than 1% per 24 h, and response time of 60 s. $SO_2$ was measured using a pulsed fluorescence $SO_2$ analyzer (Model 43C/I) with the lowest detection limit of 0.5 ppb, precision of 1% of reading or 1 ppb, zero drift of less than 1 ppb $(24\ h)^{-1}$, span drift of less than 0.5% full scale per 24 h, and response time of less than 20 s. CO was measured with a nondispersive infrared analyzer (Model 48I) with the lowest detection limit of 0.4 ppm, zero drift of less than 0.1 ppb $(24\ h)^{-1}$, span drift of less than 0.1% full scale per 24 h, and response time of less than 60 s. The $PM_{2.5}$ was measured by RP1400a TEOM micro-oscillation balance ambient particulate monitor with a resolution of 0.1 μg $m^{-3}$, a detection limit of 0.06 μg $m^{-3}$ (1-h average), and precisions of ±1.5 μg $m^{-}$

https://doi.org/10.5194/acp-2019-788
Preprint. Discussion started: 16 December 2019


Atmospheric Chemistry and Physics Discussions

$^{3}$ (1-h average) and ±0.5 μg m$^{-3}$ (24-h average). The entire system was heated to 50 °C, thus, loss of semi-volatile compounds thereby cannot be avoided. Depending on the ammonium nitrate levels and ambient temperatures, up to 25 % lower mass concentrations were found for select daily means compared with gravimetric filter measurements. The sampling methods and instrument protocols as well as quality assurance/quality control (QA/QC) procedures for air quality monitoring are described in detail in the Chinese National Environmental Protection Standard, Automated Methods for Ambient Air Quality Monitoring (HJ/T 193–2005; State Environmental Protection Administration of China, 2006). The measurement techniques are the same as those used in (Wang et al., 2014b;Xin et al., 2010).

**Volatile organic compounds** Ambient VOC samples were collected and analyzed continuously and automatically with a time resolution of 1 h using a custom-built gas chromatography-mass spectrometry/flame ionization detector (GC-MS/FID). The availability of this system for VOCs measurement are well verified and it has been used in several large field campaign (Chen et al., 2014;Yuan et al., 2013;Wu et al., 2016). The online GC-MS/FID system consisted of three major components: a cryogen-free cooling device for creating ultra-low temperatures (TH300, Wuhan Tianhong Environmental protection industry co., LTD, Wuhan, China), a sampling and preconcentration system for VOC collection and enrichment, and a gas chromatography (GC, 7820A, Agilent Technologies, Santa Clara, CA, USA) equipped with an MS and an FID (5977E, Agilent Technology, Santa Clara, CA, USA) for VOC separation and detection (Wang et al., 2014a). A complete analysis cycle for ambient VOC measurements by the online GC-MS/FID system includes five stages: preparation, sampling and preconcentration, injection/GC analysis, idle/GC analysis, and back purge/GC analysis. Briefly, moisture and $CO_2$ are removed before VOC analysis. Most C2-C5 hydrocarbons were separated on a PLOT-$Al_2O_3$ column (15 m×0.32 mm ID×3 μm, J&W Scientific, USA), and measured by the FID channel. Other compounds were separated on a semi-polar column (DB624, 60 m×0.25 mm ID×1.4 μm, J&W Scientific, USA) and quantified using a quadrupole MS detector.

The compounds analyzed were subjected to rigorous quality assurance and quality control procedures (QA/QC). The VOCs detected by FID were quantified by the external standard method,

https://doi.org/10.5194/acp-2019-788
Preprint. Discussion started: 16 December 2019


Atmospheric Chemistry and Physics Discussions

and the components detected by MS were quantified by the internal standard method. Four compounds, i.e., bromochloromethane, 1,4-difluorobenzene, chlorobenzene-d5, and bromofluorobenzene, were used as internal standards. Specifically, the system was calibrated at multiple concentrations in the range of 0.8-8 ppb by two gas standards, i.e., a mixture of 57 PAMS (provided by Spectra Gases Inc., USA), and a mixture of oxygenated VOCs (OVOCs) and halocarbons (provided by Spectra Gases Inc., USA). $R^2$ values for the calibration curves ranged from 0.941(n-Dodecane) to 1.000 for VOCs, indicating that integral areas of the peaks were proportional to concentrations of target compounds. The method detection limit (MDL) of the online GC-FID/MS system for all measured compounds ranged from 0.003 to 0.092 ppb. The measurement relative standard deviation (RSD) for measured compounds ranged from 2.1% to 14.9% (Yang et al., 2019). To check the stability of the instrument, routine calibration was performed periodically by using a calibration gas with a mixing ratio of 2 ppb consisting of 56 kinds of VOC components. The variations between the measured and nominal concentrations of the periodic calibration were within 10%. The signal variations of each targeted compound due to system instability were corrected by the signal of CFC-113 (1,1,2-trichloro-1,2,2-trifluoroethane) due to its long atmospheric lifetime and stable anthropogenic emissions (Yuan et al., 2013;Chen et al., 2014). Detailed instrumental and operational parameters are described in our previous study (Yang et al., 2019).

**Photolysis frequency** The photolysis frequencies, $J_{O^1D}$, $J_{NO_2}$ and $J_{NO_3}$, in the atmosphere are measured by the PFS-100 Photolysis Spectrometer (Juguang Technology (hangzhou) Co., Ltd, Hangzhou, China). The photolysis rate is calculated by integrating the actinic flux with the known absorption cross section $\sigma(\lambda)$ and quantum yield $\varphi(\lambda)$. The actinic flux is spherically integrated photon radiance of the solar radiation in the atmosphere. The spectrometer obtains spectral information in a certain wavelength range, which mainly uses quartz receiver to collect solar radiation from all directions, and convert it into the actinic flux $F_\lambda$. $\sigma(\lambda)$ is the absorption cross section of the species that absorbs in certain wavelength range and $\varphi(\lambda)$ is quantum yield of the photodissociation reaction product; these two coefficients have been measured by experiments and can be directly looked up and used.

https://doi.org/10.5194/acp-2019-788
Preprint. Discussion started: 16 December 2019


Atmospheric Chemistry and Physics Discussions

**Aerosol surface area density** Particle surface concentrations in the range of 10-9486.8 nm (mobility diameter, dm) were measured using WPS (Model 1000XP Wide Range Particle Spectrometer, MSP Corporation, USA). The instruments provided continuous measurements during the whole observation except for the maintenance of instruments and power outages. Ambient air was drawn into a stainless steel tube with a length of 3.0 m and an inner diameter of 0.5 inch in via a steel dust seal. From this tube, ambient air from the split flow was drawn through a conductive silicone tubing with a 1/4 inch in inner diameter via a stainless tube with a length of 0.5 cm into the WPS at rates of 1.0 L·min$^{-1}$. The overall RH was maintained below 50% by a Nafion tube to avoid water condensation within the inlet systems.

**Meteorology parameters** In addition, the meteorological parameters, including wind speed, wind direction, temperature and relative humidity were obtained from the National Meteorological Information Center (http://data.cma.cn/).

### 2.3 Speciated radical reactivity

Radical reactivity is a measure of the strength of the sinks for the radical (Sonderfeld et al., 2016;Fuchs et al., 2017a;Fuchs et al., 2017b;Tan et al., 2019). Total radical reactivity (s$^{-1}$) is defined as the total radical loss rate, which is the inverse of its lifetime with respect to a radical in the atmosphere (Di Carlo et al., 2004;Mao et al., 2009;Mao et al., 2010;Liebmann et al., 2017;Liebmann et al., 2018b). High radical reactivity values correspond to short lifetimes and long-lived species have low reactivities.

For total OH reactivity

$$R_{OH} = \sum K_{OH+VOC_i}[VOC_i] + K_{OH+CO}[CO] + K_{OH+NO}[NO] + K_{OH+NO_2}[NO_2] + K_{OH+SO_2}[SO_2] + K_{OH+O_3}[O_3] + \cdots \quad (1)$$

For total $NO_3$ reactivity

$$R_{NO_3} = \sum K_{NO_3+VOC_i}[VOC_i] + K_{NO_3+NO}[NO] + K_{NO_3+NO_2}[NO_2] + K_{NO_3+SO_2}[SO_2] + \cdots \quad (2)$$

For total $O_3$ reactivity

$$R_{O_3} = \sum K_{O_3+VOC_i}[VOC_i] + K_{O_3+NO}[NO] + K_{O_3+NO_2}[NO_2] + \cdots \quad (3)$$

https://doi.org/10.5194/acp-2019-788
Preprint. Discussion started: 16 December 2019


Atmospheric Chemistry and Physics Discussions

In the above equations, the pseudo first order rate coefficients (in $cm^3$ $molecule^{-1}$ $s^{-1}$) for OH-$VOC_i$ ($K_{OH+VOC_i}$), OH-CO ($K_{OH+CO}$), OH-NO ($K_{OH+NO}$), OH-$NO_2$ ($K_{OH+NO_2}$), OH-$SO_2$ ($K_{OH+SO_2}$), OH-$O_3$ ($K_{OH+O_3}$), $NO_3$-$VOC_i$ ($K_{NO_3+VOC_i}$), $NO_3$-NO ($K_{NO_3+NO}$), $NO_3$-$NO_2$ ($K_{NO_3+NO_2}$), $NO_3$-$SO_2$ ($K_{NO_3+SO_2}$), $O_3$-$VOC_i$ ($K_{O_3+VOC_i}$), $O_3$-NO ($K_{O_3+NO}$) and $O_3$-$NO_2$ ($K_{O_3+NO_2}$) were based on recommended values from the International Union of Pure and Applied Chemistry (IUPAC) Subcommittee for Gas Kinetic Data Evaluation (http://iupac.pole-ether.fr, last accessed: 25 July 2018), the JPL-NASA Evaluation of Chemical Kinetics and Photochemical Data for Use in Atmospheric Studies (Atkinson et al., 2004;Atkinson et al., 2006b) and the Master Chemical Mechanism, MCM v3.2 (Ferracci et al., 2018), via the website: http://mcm.leeds.ac.uk/MCM (last accessed: 25 July 2019); $[VOC_i]$, $[CO]$, $[NO]$, $[NO_2]$, $[SO_2]$ and $[O_3]$ are their concentrations (in molecules $cm^{-3}$), respectively.

**2.4 Atmospheric oxidation capacity**

The term "oxidation capacity" of an oxidant $X$ (= $NO_3$, OH and $O_3$) is defined as the sum of the respective oxidation rates of the molecules $Y_i$ (Geyer et al., 2001).

$$\mathrm{AOC} = \sum_{i=1} k_{Y_i-X}[Y_i]\,[X] = \sum_{i=1} R_X^{Y_i}\,[X] \quad (4)$$

Here, $[Y_i]$ and $[X]$ are mixing ratios of molecule $Y_i$ and oxidant $X$, respectively. $k_{Y_i-X}$ is the rate constant of the molecule $Y_i$ with oxidant $X$. $R_X^{Y_i}$ is the oxidant $X$ reactivity of molecules $Y_i$.

Simultaneous measurements of OH and $NO_3$ are not available in this study. The OH radical concentration (in molecule $cm^{-3}$) can be estimated using the expression for the dependence of the OH concentration on solar UV and $NO_2$ suggested by (Ehhalt and Rohrer, 2000) and verified by (Alicke, 2002):

$$[OH] = \mathrm{a} \times (J_{O^1D})^{\alpha} \times (J_{NO_2})^{\beta} \times \frac{b \times [NO_2] + 1}{c \times [NO_2]^2 + d \times [NO_2] + 1} \quad (5)$$

Here, $J_{O^1D}$ and $J_{NO_2}$ are the measured photolysis frequencies ($s^{-1}$) of $O_3$ and $NO_2$, respectively. The values of $\alpha = 0.83$, $\beta$=0.19, a=$4.1\times10^9$, b=140, c=0.41 and d=1.7 are obtained from measurement data with $NO_x$ concentrations > 1 ppb during the POPCORN campaign at a rural site in Germany.

https://doi.org/10.5194/acp-2019-788
Preprint. Discussion started: 16 December 2019


Atmospheric Chemistry and Physics Discussions

297 The $NO_3$ concentration (in molecule $cm^{-3}$) could be determined based on the steady-state
298 assumption of the $NO_3$ concentration in the atmosphere (Yuan et al., 2013):

299 $$[NO_3] = \frac{k_{NO_2+O_3} \times [NO_2] \times [O_3]}{J_{NO_3} + k_{NO+NO_3} \times [NO] + R_{NO_3}^{VOCs} + K_{eq} \times \frac{\gamma \bar{c} A}{4} \times [NO_2]} \quad (6)$$

300 Here, $J_{NO_3}$ is the measured photolysis frequency ($s^{-1}$) of $NO_3$. $R_{NO_3}^{VOCs}$ ($s^{-1}$) is the VOC
301 reactivity to $NO_3$. The rate coefficients for $NO_2$-$O_3$ ($k_{NO_2+O_3}$) and NO-$NO_3$ ($k_{NO+NO_3}$) were taken
302 from the JPL-NASA Evaluation of Chemical Kinetics and Photochemical Data for Use in
303 Atmospheric Studies (Atkinson et al., 2004) and are $3.5\times10^{-17}$ and $2.6\times10^{-11}$ $cm^3$ $molecule^{-1}$ $s^{-1}$,
304 respectively. $K_{eq}$ (=$3.26\times10^{-11}$ $cm^3$ $molecule^{-1}$ $s^{-1}$ at 298K) is the equilibrium constant for $NO_3$
305 +$NO_2$ +M⇆$N_2O_5$ +M (Atkinson et al., 1986). $\gamma$ (=0.022) is the dimensionless uptake coefficient
306 obtained in North China Plain (Tham et al., 2018). $\bar{c}$ is the mean molecular velocity of $N_2O_5$
307 (26233cm $s^{-1}$ at 298 K). A is the aerosol surface area density ($cm^2$ $cm^{-3}$). However, simultaneous
308 measurement of aerosol surface area density with VOC is not available in this study. We calculated
309 the aerosol surface area density at the site on a linear fitting equation (aerosol surface area density
310 =415.32×[$PM_{2.5}$]+6511.6 $R^2$=0.7846 p<0.001) between aerosol surface area density and $PM_{2.5}$
311 measured from 1 to 22 November 2018 , as showed in Figure S1. Figure S2 shows the time series
312 of calculated aerosol surface area density. The campaign-averaged values of aerosol surface area
313 density was $2.35\times10^{-6}$ $cm^2$ $cm^{-3}$ with a range of $7.21\times10^{-7}$- $5.48\times10^{-6}$ $cm^2$ $cm^{-3}$.
314
315 **3 Results and discussion**
316 **3.1 Overview of measurements**
317 For the data evaluation, all measurements were averaged over 1-hour time intervals. The measured
318 concentrations of major pollutants and meteorological parameters at Xianghe are depicted in Figure
319 2, while the mean diurnal profiles are shown in Figure S3. During the campaign, sunny weather
320 conditions prevailed with temperatures ranging from 25℃ to 31℃ during the daytime. The ambient

https://doi.org/10.5194/acp-2019-788
Preprint. Discussion started: 16 December 2019


Atmospheric Chemistry and Physics Discussions

temperature was comparable with those measured in Beijing (02 Jul-19 Jul 2014), Shanghai (21 Aug-02 Sep 2016), and Chongqing (27 Aug-04 Sep 2015), but higher than that in Guangzhou (23-31 Oct 2015) (Tan et al., 2019). Wind data suggested that the prevailing wind was from the eastern sampling site with a mean wind speed of 1.0 m $s^{-1}$ ranging from 0.3 m $s^{-1}$ to 1.4 m $s^{-1}$, and the average relative humidity was 85%, reaching up to 96% during the night (Figure 2). For the campaign, $NO_y$ showed a morning peak with a maximum of 228.8 ppb at 9:00 h and an afternoon dip with a minimum of 26.1 ppb at 16:00 h (Figure S3a). Campaign-averaged data maximum and minimum $SO_2$ mixing ratios of 3.6 ppb at approximately 14:00 h and 2.3 ppb during nighttime were obtained (Figure S3c). For $J_{O^1D}$, $J_{NO_2}$ and $J_{NO_3}$, a similar maximum at ~14:00 h was observed, with maximum values of 2.1 ×$10^{-5}$ $s^{-1}$, 5.3 ×$10^{-3}$ $s^{-1}$ and 1.3 ×$10^{-1}$ $s^{-1}$, respectively (Figure S3g-Figure S3i). The maximum of $J_{O^1D}$ at this site was comparable with that in Shanghai and Chongqing but higher than that in Guangzhou and lower than that in Beijing (Tan et al., 2019;Wang et al., 2019a). The observed mean daily maxima of $J_{NO_2}$ at this site were higher than those observed in the eastern Mediterranean (Gerasopoulos et al., 2012) but lower than that in Beijing (Wang et al., 2019a).

The diurnal maximum $O_3$ concentration was 72 ppb at this site (Figure S3d), which was in line with that observed in Beijing (72 ppb) but higher than that measured in Guangzhou (65 ppb) and Chongqing (56 ppb) and lower than that observed in Shanghai (80 ppb) (Tan et al., 2019). The $O_3$ precursors, CO, $NO_x$, and VOCs, are shown in Figure 2 and Figure S3. As expected, with the accumulation of CO, $NO_x$, and VOCs, the $O_3$ concentration gradually increases, and the concentration of VOCs gradually decreases as the photochemical reaction progresses (Kansal, 2009;Song et al., 2018). CO and $NO_x$ showed a similar diurnal profile with a maximum during the rush hour and a minimum in the afternoon (Figure S3b and Figure S3e), suggesting that both CO and $NO_x$ originated from the same source (enhanced traffic emission), and/or were manipulated by the same factor (e.g., poor dilution conditions). During the campaign, the average mixing ratio of total VOCs was 25.3 ppb, with the highest contributions from alkanes (13.2 ppb, 51.4%), followed by OVOCs (4.9 ppb, 19.8%), aromatics (4.3 ppb, 16.7%) and alkenes (3.0 ppb, 12.1%). The top 10 species (Figure 3a), in terms of emissions, consisted of propane (3.7 ppb), acetone (3.2 ppb), ethane (3.2 ppb), n-butane (1.9 ppb), m/p-Xylene (1.6 ppb), iso-pentane (1.3 ppb), ethylene (1.3 ppb), iso-butane (1.1 ppb), isoprene (1.0 ppb) and n-pentane (0.7 ppb), accounting for a total of 75.1% of the

https://doi.org/10.5194/acp-2019-788
Preprint. Discussion started: 16 December 2019


Atmospheric Chemistry and Physics Discussions

TVOC concentration. As typical tracers of vehicle-related emissions, propane, ethane, ethene, butanes and pentanes were present in high concentrations, suggesting that vehicle-related emissions were likely to be the dominant source of VOCs at this site. In addition, the shape of diurnal variations of TVOCs backed the presence of vehicle-related emissions, which presented relatively higher mixing ratios during the early morning and from evening to midnight, which may be related to enhanced traffic emissions during rush hours and poor dilution conditions (Yuan et al., 2009;He et al., 2019;Tan et al., 2019). On the other hand, the mixing ratios of TVOCs began to decrease at 10:00 h and maintained a broad trough during daytime hours probably due to the increased photochemical removal processes favoring the destruction of VOCs, elevated planetary boundary layer (PBL) advancing the dispersion of VOCs and/or less VOC emissions reducing levels of VOCs (He et al., 2019;Zheng et al., 2018). In contrast, the OVOC concentrations (not shown) increased from a minimum near sunrise and a maximum in the late afternoon, reflecting the accumulation of OVOCs during the photochemically active period of the day and illustrating the time profile of formation for a secondary species (Yuan et al., 2012).

### 3.2 Reactivity of hydroxy radical, nitrate radical and ozone

In this study, $R_{OH}^{\text{calculated}}$, $R_{NO_3}^{\text{calculated}}$ and $R_{O_3}^{\text{calculated}}$ were comprehensively conducted. All the reactivity values discussed in this study were calculated rather than observed. Figure 4 shows the time series of calculated $R_{OH}^{\text{calculated}}$, $R_{NO_3}^{\text{calculated}}$ and $R_{O_3}^{\text{calculated}}$. The contributions of different atmospheric compounds to $R_{OH}$ are presented in Figure 5. The mean diurnal variations in $R_{OH}^{\text{calculated}}$, $R_{NO_3}^{\text{calculated}}$ and $R_{O_3}^{\text{calculated}}$ are shown in Figure 6 and Figure 7. The frequency distributions of $R_{OH}^{\text{calculated}}$, $R_{NO_3}^{\text{calculated}}$ and $R_{O_3}^{\text{calculated}}$ are depicted in Figure S4-Figure S9.

#### 3.2.1 OH reactivity ($R_{OH}$)

The $R_{OH}$ of trace gases was categorized into $SO_2$, CO, $NO_x$ (sum of NO and $NO_2$) and TVOCs, which were grouped into alkanes, alkenes, aromatics, OVOCs and isoprene (Table S1 lists the VOCs included in each group), as shown in Figure 4a and 4b. The total $R_{OH}$, $R_{OH}^{\text{total}}$, was between 8.5 and 68.1 $s^{-1}$, with an average of 25.6±9.7 $s^{-1}$ (± standard deviation). Statistically, the average $R_{OH}^{\text{total}}$ was much higher than those determined in Beijing (16.4 $s^{-1}$/20±11 $s^{-1}$) (Tan et al., 2019;Yang et al., 2017), Shanghai (13.5 $s^{-1}$) (Tan et al., 2019), Chongqing (17.8 $s^{-1}$) (Tan et al., 2019), Jinan (19.4±2.1

https://doi.org/10.5194/acp-2019-788
Preprint. Discussion started: 16 December 2019


Atmospheric Chemistry and Physics Discussions

381 $s^{-1}$) (Lyu et al., 2019), Wangdu (10-20 $s^{-1}$) (Fuchs et al., 2017b), Houston (9-22 $s^{-1}$) (Mao et al.,
382 2010), London (18.1 $s^{-1}$) (Whalley et al., 2016) and Nashville (11.3 ± 4.8 $s^{-1}$) (Kovacs et al., 2003)
383 but was comparable or lower than those in Guangzhou (22.7 $s^{-1}$) (Tan et al., 2019), Heshan (31±20
384 $s^{-1}$) (Yang et al., 2017), Backgarden (mean maximum value of 50 $s^{-1}$) (Lou et al., 2010) and New
385 York (25 $s^{-1}$) (Ren et al., 2006b). The $R_{OH}^{\text{total}}$ was mainly contributed by $NO_x$ (12.0±7.1 $s^{-1}$, 47%),
386 followed by CO (7.2±2.6 $s^{-1}$, 28%) and TVOCs (6.2±4.6 $s^{-1}$, 24%) and to a lesser extent by $SO_2$
387 and $O_3$ (0.2±0.1 $s^{-1}$, 1%), indicating the strong influence of anthropogenic emissions in Xianghe.
388 The majority of $R_{OH}^{\text{total}}$ values were below 20 $s^{-1}$, as seen in the frequency distribution, which was
389 dominated by the sum of low $R_{OH}$ contributions and less by single compounds with high $R_{OH}$
390 (Figure S4a-S4e), highlighting the necessity of considering a large number of species to obtain a
391 complete picture of $R_{OH}^{\text{total}}$. Specifically, the cumulative frequency distribution (Figure S5a) clearly
392 showed that the $R_{OH}^{\text{total}}$ at values >40 $s^{-1}$ was dominated entirely by $R_{OH}^{NO_x}$, and the $R_{OH}^{\text{total}}$ at values
393 between 20-40 $s^{-1}$ was nearly dominated by $R_{OH}^{NO_x}$ and $R_{OH}^{\text{VOCs}}$.
394
395 Figure 5 presents the contributions from different atmospheric constituents, including CO, NOx, the
396 sum of nonmethane hydrocarbons (NMHC), OVOCs and the sum of biogenic VOC (BVOCs), to to
397 the $R_{OH}$ for 12 different urban atmospheric measurements around the world and different periods
398 of the year. In total, the contributions from the inorganic species (CO and $NO_x$) exceeded 50% for
399 Xianghe, Beijing (Tan et al., 2019), Shanghai (Tan et al., 2019), Guangzhou (Tan et al., 2019),
400 Chongqing (Tan et al., 2019), Heshan (Yang et al., 2017), Paris (Dolgorouky et al., 2012), Tokyo
401 (Yoshino et al., 2006) and New York (Mao et al., 2010), showing the large influence of traffic-
402 related emissions on $R_{OH}^{\text{total}}$. The contributions from CO and $NO_x$ were very similar in Xianghe
403 (75%) and Paris (76%), although different seasons are considered, suggesting a possible influence
404 from traffic emissions (Dolgorouky et al., 2012). In contrast, the NMHCs contributed between 12%
405 and 28% to the $R_{OH}^{\text{total}}$ in these cities. However, the contributions from CO and $NO_x$ in Mexico City
406 and Houston (Mao et al., 2010) were only 37% and 29%, respectively, but the contributions from
407 the NMHCs reached 51% and 46%, respectively. This was accounted for by (1) Mexico City sharing
408 high NMHC due to higher biomass fuel being burned (de Gouw et al., 2006) and (2) higher
409 contributions from aromatics due to high industrial solvent emissions in Houston (Leuchner and
410 Rappenglück, 2010). In conclusion, the $R_{OH}$ was a typical fingerprint of anthropogenic emissions

https://doi.org/10.5194/acp-2019-788
Preprint. Discussion started: 16 December 2019


Atmospheric Chemistry and Physics Discussions

(traffic-related emissions or industrial emissions), although comparing $R_{OH}$ in different places is a limited exercise because they are by nature a point measurement that can vary inside the same city depending on the geographic location of the measurement and the season (Dolgorouky et al., 2012).

The $R_{OH}$ of TVOCs, $R_{OH}^{\mathrm{TVOCs}}$, was 6.2±4.6 $s^{-1}$, which was much lower than those in Beijing (11.2 $s^{-1}$) and Heshan (18.3 $s^{-1}$) (Yang et al., 2017) due to the higher content of reactive hydrocarbons (e.g., alkenes and aromatics) in Beijing and Heshan and the unmeasured species (e.g., HCHO and acetaldehyde) in this study. Isoprene (2.5±3.7 $s^{-1}$, 40%) dominated over aromatics (1.5±1.7 $s^{-1}$, 24%), alkenes (0.9±0.8 $s^{-1}$, 14%), OVOCs (0.7±0.8 $s^{-1}$, 12%) and alkanes (0.7±0.5 $s^{-1}$, 10%) in the $R_{OH}^{\mathrm{TVOCs}}$. The majority of $R_{OH}^{\mathrm{VOCs}}$ values were below 2 $s^{-1}$ (Figure S6a-S6e). The cumulative frequency distribution showed that $R_{OH}^{\mathrm{TVOCs}}$ at values of >15 $s^{-1}$ was dominated entirely by $R_{OH}^{\mathrm{isoprene}}$, the $R_{OH}^{\mathrm{TVOCs}}$ at values between 10-15 $s^{-1}$ was dominated by $R_{OH}^{\mathrm{isoprene}}$ and $R_{OH}^{\mathrm{aromatics}}$, and the $R_{OH}^{\mathrm{TVOCs}}$ at values between 5-10 $s^{-1}$ was nearly dominated by $R_{OH}^{\mathrm{isoprene}}$, $R_{OH}^{\mathrm{aromatics}}$ and $R_{OH}^{\mathrm{OVOCs}}$ (Figure S7). Alkanes accounted for >50% of the mixing ratio of VOCs, but only 10% of the $R_{OH}^{\mathrm{TVOCs}}$. In contrast, aromatics, alkenes and OVOCs accounted for 44.6% of the mixing ratio of VOCs, providing 50% of the $R_{OH}^{\mathrm{TVOCs}}$. Significantly, isoprene accounted for only 4% of the mixing ratio of VOCs but provided 40% of the $R_{OH}^{\mathrm{TVOCs}}$. This was explained by (1) the relatively low concentration of aromatics, alkenes and OVOCs measured during the campaign, (2) the relatively high concentration of isoprene and (3) the generally large isoprene reaction rate coefficients with OH ($101\times10^{-12}$ $cm^3$ $molecule^{-1}$ $s^{-1}$) (Atkinson et al., 2006a). The $R_{OH}$ from isoprene in this study was much higher than those in Guangzhou (0.4 $s^{-1}$), Beijing (1 $s^{-1}$), Chongqing (1 $s^{-1}$) (Tan et al., 2019) and Heshan (0.9 $s^{-1}$) (Yang et al., 2017). The $R_{OH}$ from alkenes, aromatics and OVOCs were dominated by m/p-xylene (0.8±0.9 $s^{-1}$), ethylene (0.3±0.2 $s^{-1}$), hexanal (0.2±0.4 $s^{-1}$), o-xylene (0.2±0.3 $s^{-1}$), propylene (0.2±0.2 $s^{-1}$) and styrene (0.2±0.6 $s^{-1}$) (Figure 3b). In total, these 6 species contributed 31% of the $R_{OH}^{\mathrm{TVOCs}}$ from 17% of the TVOC emissions.

The mean diurnal profiles of the $R_{OH}$ of trace gases and VOC groups are presented in Figure 6a-6e and Figure 7a-7e, respectively. In general, the $R_{OH}^{\mathrm{total}}$ was the lowest in the afternoon and the highest during rush hours, reaching a maximum of 31 $s^{-1}$ during the morning rush hour and a night-time peak of 28 $s^{-1}$ (Figure 6a). Most campaigns have also reported a slightly higher $R_{OH}$ in the

https://doi.org/10.5194/acp-2019-788
Preprint. Discussion started: 16 December 2019


Atmospheric Chemistry and Physics Discussions

morning traffic rush hour, which can be explained by higher levels of reactive gases such as NO and VOCs due to heavy traffic, as well as slower reactions (Yang et al., 2016;Dolgorouky et al., 2012;Fuchs et al., 2017b;Mao et al., 2010;Ren, 2003;Ren et al., 2006a;Williams et al., 2016). A similar diurnal profile was also observed for contributions from $NO_x$, CO, alkane, alkene and aromatic species, which are typically connected to emissions from anthropogenic activities. The shape of the $R_{OH}^{\text{total}}$ diurnal pattern was slightly shifted to the $R_{OH}^{NO_x}$, strengthening the idea that the local pollution in Xianghe was possibly impacted by traffic emissions. However, a different diurnal behavior to that of the above species was observed for OVOCs (Figure 7d) and isoprene (Figure 7e), which is emitted by plants or photochemical production. The $R_{OH}$ from OVOCs increased by a factor of approximately 1.6 from nighttime to daytime, suggesting that during the daytime, dilution or chemical removal had a weaker influence on the observed OVOCs than fresh production by photochemistry. The opposite diurnal variation was reported in Wangdu, which showed a weak diurnal variation with a decrease by a factor of approximately 2 from the morning to the evening (Fuchs et al., 2017b). Biogenic isoprene is dependent on temperature and light intensity (Guenther et al., 1993;Pacifico et al., 2009;Saunier et al., 2017;Ding et al., 2014) and anthropogenic isoprene is predominantly emitted by road traffic (Derwent et al., 1995;Ye et al., 1997); hence, the $R_{OH}$ from isoprene increased during the daytime, with a morning peak of 3 $s^{-1}$ at 10:00 h and a night-time peak of 7 $s^{-1}$ at 19:00 h. Many rainforest campaigns have also reported a significant diurnal pattern with higher $R_{OH}$ from isoprene and OVOCs at noontime or reached a maximum at the beginning of the night (Edwards et al., 2013;Sinha et al., 2008;Yang et al., 2016;Zannoni et al., 2016;Bsaibes et al., 2019;Kaiser et al., 2016;Ramasamy et al., 2016). Notably, the large amplitude of standard deviation bars highlighted the large diel variability.

### 3.2.2 $NO_3$ reactivity ($R_{NO_3}$)

The $R_{NO_3}$ of trace gases was categorized into $SO_2$, $NO_x$ and TVOCs which were grouped into alkanes, alkenes, aromatics, OVOCs and isoprene (Table S1 lists the VOCs included in each group), as shown in Figure 4c and 4d. Campaign-averaged values of $R_{NO_3}^{\text{total}}$ were 2.2±2.6 $s^{-1}$ (± standard deviation) ranging from as low as 0.7 $s^{-1}$ to as high as 27.5 $s^{-1}$. The average $R_{NO_3}^{\text{total}}$ was much higher than those determined during the IBAIRN campaign (Influence of Biosphere-Atmosphere Interactions on the Reactive Nitrogen budget) (Liebmann et al., 2018a) and at a rural mountain site

https://doi.org/10.5194/acp-2019-788
Preprint. Discussion started: 16 December 2019


Atmospheric Chemistry and Physics Discussions

(988 m a.s.l.) in southern Germany in 2017 (Liebmann et al., 2018b) due to the higher contributions from $NO_x$ in this study. We noted that $NO_x$ was by far the main contributors to the $R_{NO_3}^{\text{total}}$, representing 99% of the $R_{NO_3}^{\text{total}}$ on average. NO exhibited the most prominent contribution to the $R_{NO_3}^{\text{total}}$ and represented an average of 78% of the $R_{NO_3}^{\text{total}}$. In comparison to NO, $NO_2$ had a maximum contribution during night-time and represented, on average, 27% of the $R_{NO_3}^{\text{total}}$. The $R_{NO_3}$ of VOCs and $SO_2$ was very minor, with no more than 1% of the $R_{NO_3}^{\text{total}}$ over the whole campaign. The majority of $R_{NO_3}^{\text{total}}$ values were below 5 $s^{-1}$, but below $5\times10^{-2}$ $s^{-1}$, 5 $s^{-1}$, $5\times10^{-9}$ $s^{-1}$ for $R_{NO_3}^{\text{TVOCs}}$, $R_{NO_3}^{NO_x}$ and $R_{NO_3}^{SO_2}$, respectively, as seen in the frequency distribution (Figure S4f-S4i). The cumulative frequency distribution clearly showed that the $R_{NO_3}^{\text{total}}$ at low and high values was entirely dominated by $R_{NO_3}^{\text{TVOCs}}$ and $R_{NO_3}^{NO_x}$, respectively (Figure S5b).

The $R_{NO_3}$ of TVOCs, $R_{NO_3}^{\text{TVOCs}}$, was $2.2\pm2.7\times10^{-2}$ $s^{-1}$ on average with a minimum of $1.0\times10^{-3}$ $s^{-1}$ and a maximum of 0.2 $s^{-1}$. The largest fraction of attributed $R_{NO_3}^{\text{TVOCs}}$ was provided by isoprene (77%), followed by aromatics (15%), alkene (7%) and OVOCs (1%). The measured alkanes played virtually no role for $R_{NO_3}^{\text{TVOCs}}$, although they accounted for more than 50% of the mixing ratio of VOCs. This can be largely explain by the fact that the reaction rate coefficients of isoprene, aromatics, alkene and OVOCs with $NO_3$ are 1-5 orders of magnitude higher than the alkane reaction rate coefficients with $NO_3$ (Atkinson et al., 2006b;Atkinson and Arey, 2003;Yuan et al., 2013;Ferracci et al., 2018;Jenkin et al., 2015). The majority of $R_{NO_3}^{\text{alkanes}}$, $R_{NO_3}^{\text{alkenes}}$, $R_{NO_3}^{\text{aromatics}}$, $R_{NO_3}^{\text{OVOCs}}$ and $R_{NO_3}^{\text{isoprene}}$ are below $5.0\times10^{-5}$ $s^{-1}$, $3.0\times10^{-3}$ $s^{-1}$, $1.0\times10^{-2}$ $s^{-1}$, $1.0\times10^{-3}$ $s^{-1}$ and $1.0\times10^{-3}$ $s^{-1}$, respectively (Figure S6f-S6j). The cumulative frequency distribution showed that $R_{NO_3}^{\text{TVOCs}}$ at values of > 0.1 $s^{-1}$ was entirely dominated by $R_{NO_3}^{\text{isoprene}}$, the $R_{NO_3}^{\text{TVOCs}}$ at values between 0.01-0.1 $s^{-1}$ was dominated by $R_{NO_3}^{\text{isoprene}}$ and $R_{NO_3}^{\text{aromatics}}$, and the $R_{NO_3}^{\text{TVOCs}}$ at values of $<1.0\times10^{-5}$ $s^{-1}$ was entirely dominated by $R_{NO_3}^{\text{alkanes}}$ (Figure S8). The top seven species in terms of $R_{NO_3}^{\text{TVOCs}}$ consisted of styrene, cis-2-butene, trans-2-butene, cis-2-pentene, hexanal, propylene and 1,3-butadiene (Figure 3c). These species contributed only 4% to VOC emissions but accounted for 50% of the $R_{NO_3}^{\text{TVOCs}}$.

https://doi.org/10.5194/acp-2019-788
Preprint. Discussion started: 16 December 2019


Atmospheric Chemistry and Physics Discussions

499 $R_{NO_3}^{\text{total}}$ displayed a weak diel variation with a campaign-averaged morning peak value of 4.0$s^{-1}$ at
500 6:00-7:00 h (Figure 6f). The diurnal profile of $R_{NO_3}^{NO_x}$ (Figure 6h) appears to be the major driver for
501 the diurnal profile of $R_{NO_3}^{\text{total}}$. The morning peak value of $R_{NO_3}^{\text{total}}$ could be explained by the
502 accumulation of $NO_x$ due to traffic emissions that are released into the shallow nocturnal boundary
503 layer during the morning rush hours. In contrast, the average diurnal profile of $R_{NO_3}^{\text{TVOCs}}$ (Figure 6g)
504 had a maximum at 19:00 h, which was slightly shifted to $R_{NO_3}^{\text{isoprene}}$ (Figure 6j). The evening peak
505 value of $R_{NO_3}^{\text{TVOCs}}$ could be accounted for by the accumulation of isoprene due to vegetation
506 emissions and traffic emissions that are released into the shallow nocturnal boundary layer. $R_{NO_3}^{\text{alkanes}}$
507 (Figure 7f), $R_{NO_3}^{\text{alkenes}}$ (Figure 7g), $R_{NO_3}^{\text{aromatics}}$ (Figure 7h), $R_{NO_3}^{\text{OVOCs}}$ (Figure 7i) and $R_{NO_3}^{SO_2}$
508 (Figure 6i) played virtually no roles in the diurnal variations of $R_{NO_3}^{\text{total}}$ and $R_{NO_3}^{\text{TVOCs}}$, although they
509 exhibited a more distinct diurnal profile.
510
511 **3.2.3 $O_3$ reactivity ($R_{O_3}$)**
512 The $R_{O_3}$ of trace gases was categorized into $NO_x$ and TVOCs which were grouped into alkanes,
513 alkenes, aromatics, OVOCs and isoprene (Table S1 lists the VOCs included in each group), as
514 shown in Figure 4e and 4f. The $R_{O_3}^{\text{total}}$ at the site varied between a minimum of $3.3\times10^{-4}$ $s^{-1}$ and a
515 maximum of $1.8\times10^{-2}$ $s^{-1}$ and was $1.2\pm1.7\times10^{-3}$ $s^{-1}$ (± standard deviation) on average. NO exhibited
516 the most prominent contribution to the $R_{O_3}^{\text{total}}$ and represented on average >99% of the $R_{O_3}^{\text{total}}$,
517 whereas nearly all other contributions were < 1%. This result can be largely accounted for by the
518 generally large NO reaction rate coefficients with $O_3$ ($1.8\times10^{-14}$ $cm^3$ $molecule^{-1}$ $s^{-1}$) (Atkinson et
519 al., 2006a), which are 3, >9, 2-4, >6, 4-6 and 3 orders of magnitude higher than the $NO_2$, alkanes,
520 alkenes, aromatics, OVOCs and isoprene reaction rate coefficients with $NO_3$, respectively (Atkinson
521 et al., 2006b;Atkinson and Arey, 2003;Yuan et al., 2013;Ferracci et al., 2018;Jenkin et al., 2015).
522 The majority of $R_{O_3}^{\text{total}}$ values were below $2\times10^{-3}$ $s^{-1}$ but below $2\times10^{-6}$ $s^{-1}$ and $2\times10^{-3}$ $s^{-1}$ for
523 $R_{O_3}^{\text{TVOCs}}$ and $R_{O_3}^{NO_x}$, respectively, as seen in the frequency distribution (Figure S4j-S4l). The
524 cumulative frequency distribution clearly showed that the $R_{O_3}^{\text{total}}$ at low and high values was entirely
525 dominated by $R_{O_3}^{\text{TVOCs}}$ and $R_{O_3}^{NO_x}$, respectively (Figure S5c).
526

https://doi.org/10.5194/acp-2019-788
Preprint. Discussion started: 16 December 2019


Atmospheric Chemistry and Physics Discussions

The $R_{O_3}$ of TVOCs, $R_{O_3}^{\mathrm{TVOCs}}$, was 1.1±0.8×10$^{-6}$ s$^{-1}$ on average ranging from a minimum of 2.5×10$^{-7}$ s$^{-1}$ to a maximum of 1.0×10$^{-5}$ s$^{-1}$. Alkenes clearly dominated the $R_{O_3}^{\mathrm{TVOCs}}$ with campaign-averaged contributions of 66%. Isoprene was the second largest contributor, comprising an average of 28% of the $R_{O_3}^{\mathrm{TVOCs}}$. In comparison, aromatics and OVOCs only accounted for 5% and 1%, respectively, of the $R_{O_3}^{\mathrm{TVOCs}}$. In contrast, the measured alkanes played nearly no role for $R_{O_3}^{\mathrm{TVOCs}}$ due to their small reaction rate coefficients with $O_3$ (<1.0×10$^{-23}$ cm$^3$ molecule$^{-1}$ s$^{-1}$) (Atkinson and Arey, 2003;Atkinson et al., 2006b). The majority of $R_{O_3}^{\mathrm{alkanes}}$, $R_{O_3}^{\mathrm{alkenes}}$, $R_{O_3}^{\mathrm{aromatics}}$, $R_{O_3}^{\mathrm{OVOCs}}$ and $R_{O_3}^{\mathrm{isoprene}}$ were below 5.0×10$^{-12}$ s$^{-1}$, 2.0×10$^{-6}$ s$^{-1}$, 2.0×10$^{-7}$ s$^{-1}$, 2.0×10$^{-8}$ s$^{-1}$ and 2.0×10$^{-6}$ s$^{-1}$, respectively (Figure S6k-S6o). The cumulative frequency distribution (Figure S9) clearly showed that the $R_{O_3}^{\mathrm{TVOCs}}$ at >1.0×10$^{-7}$ was dominated by $R_{O_3}^{\mathrm{alkenes}}$, $R_{O_3}^{\mathrm{aromatics}}$ and $R_{O_3}^{\mathrm{isoprene}}$, the $R_{O_3}^{\mathrm{TVOCs}}$ between 1.0×10$^{-9}$ and 1.0×10$^{-7}$ was dominated by $R_{O_3}^{\mathrm{aromatics}}$, $R_{O_3}^{\mathrm{isoprene}}$ and $R_{O_3}^{\mathrm{OVOCs}}$, and the $R_{O_3}^{\mathrm{TVOCs}}$ <1.0×10$^{-11}$ was entirely dominated by $R_{O_3}^{\mathrm{alkanes}}$. In terms of individual species, cis-2-butene, trans-2-butene, propylene, cis-2-pentene, styrene, ethylene and 1-butene were the top seven species (Figure 3d), accounting for 25%, 20%, 7%, 6%, 5%, 5% and 3%, respectively, of the $R_{O_3}^{\mathrm{TVOCs}}$ and 0.4%, 0.2%, 1.2%, 0.1%, 0.5%, 5.3% and 0.5%, respectively, of the TVOC emissions.

Compared with $R_{OH}$ and $R_{NO_3}$, $R_{O_3}$ displayed a much weaker diel variation, especially $R_{O_3}^{\mathrm{alkenes}}$ and $R_{O_3}^{\mathrm{aromatics}}$, as shown in Figure 6 and Figure 7. This can be explained by the following reasons. First, for the same species, the reaction rate coefficients with $O_3$ were much smaller than its corresponding reaction rate coefficients with OH and $NO_3$. For example, the ethylene reaction rate coefficients with OH (8.52×10$^{-12}$ cm$^3$ molecule$^{-1}$ s$^{-1}$) and $NO_3$ (2.05×10$^{-16}$ cm$^3$ molecule$^{-1}$ s$^{-1}$) are 6 and 2 orders of magnitude higher, respectively, than the ethylene reaction rate coefficients with $O_3$ (1.59×10$^{-18}$ cm$^3$ molecule$^{-1}$ s$^{-1}$) (Atkinson and Arey, 2003;Atkinson et al., 2006b). Second, the high-emissions species reaction rate coefficients with $O_3$ are smaller than the low-emissions species reaction rate coefficients with $O_3$. For instance, the m/p-xylene (one of the top five emissions species) reaction rate coefficients with $O_3$ (<1.0×10$^{-20}$ cm$^3$ molecule$^{-1}$ s$^{-1}$) are much smaller than the 1-hexene (one of the bottom five emissions species) reaction rate coefficients with $O_3$ (1.13×10$^{-17}$ cm$^3$ molecule$^{-1}$ s$^{-1}$) (Atkinson and Arey, 2003;Atkinson et al., 2006b). The above two facets largely

https://doi.org/10.5194/acp-2019-788
Preprint. Discussion started: 16 December 2019


Atmospheric Chemistry and Physics Discussions

weaken the diurnal variation in $R_{O_3}$.

### 3.3 $R_{OH}$ and $O_3$ production regimes

Photochemical formation is the main source of ground-level $O_3$, and VOCs, CO and $NO_x$ are key precursors of tropospheric $O_3$ (Atkinson, 2000;Lyu et al., 2019). The production of $O_3$ is generally limited by VOCs or $NO_x$ or is colimited by both VOCs and $NO_x$ (Lu et al., 2010;Tang et al., 2012;Li et al., 2019a). However, $O_3$ formation is neither linearly dependent on $NO_x$ concentration nor VOC reactivity (Pfannerstill et al., 2019); reductions in the emissions of these precursors can decrease, increase, or leave the rate of $O_3$ production unchanged (Pusede and Cohen, 2012).

$R_{OH}^{\mathrm{VOCs}}$ and $R_{OH}^{\mathrm{NO}_x}$ are ways of defining $O_3$ production regimes (Kirchner et al., 2001;Lyu et al., 2019;Pfannerstill et al., 2019;Sinha et al., 2012). In this study, we use the ratio of $R_{OH}^{\mathrm{VOCs}}$ and $R_{OH}^{\mathrm{NO}_x}$, known as the s=$R_{OH}^{\mathrm{VOCs}}/R_{OH}^{\mathrm{NO}_x}$ ratio, to evaluate the $O_3$ production sensitivity, as suggested by (Kirchner et al., 2001). The thresholds of the $R_{OH}^{\mathrm{VOCs}}/R_{OH}^{\mathrm{NO}_x}$ ratios are 0.2 and 0.01. When s > 0.2 indicates VOC limitation, 0.01<s<0.2 is colimited by both VOCs and $NO_x$, and s < 0.01 $NO_x$ limitation. The $O_3$ production regime plot (Figure 8) showed that Xianghe was characterized by a strong VOC limitation. Here, 84% of the datapoints fall within the regime of VOC limitation, whereas 16% are colimited by both VOCs and $NO_x$. The higher the $O_3$ concentration is, the more obvious the VOC limitation will be. The lower the $O_3$ concentration is, the more obvious the colimited by both VOCs and $NO_x$ will be. Previous studies based on space-based HCHO/$NO_2$ column ratio (Tang et al., 2012) and VOC / $NO_x$ ratio (Wang et al., 2014b) also found that summer $O_3$ production in this district may be under a VOC-limited regime. In addition, as VOCs generally have good correlations with CO and play a similar role as CO in photochemical $O_3$ production (Atkinson, 2000). A scatter plot of CO-$NO_y$ can also be used to evaluate the $O_3$-$NO_x$-VOC sensitivity (Ding et al., 2013). Figure S10 depicts the scatter plots of CO-$NO_y$ color-coded with $O_3$ concentrations. The results showed that high $O_3$ levels are generally associated with a high CO/$NO_y$ ratio, indicating a VOC-limited regime of $O_3$ formation in Xianghe. Generally, our results suggested that control of VOCs would be most effective for controlling $O_3$ in Xianghe.

https://doi.org/10.5194/acp-2019-788
Preprint. Discussion started: 16 December 2019


Atmospheric Chemistry and Physics Discussions

### 3.4 Implications for $R_{OH}$, $R_{NO_3}$ and $R_{O_3}$-based VOC control strategies

Table 1 lists the top 10 VOC species (excluded isoprene) in terms of concentrations, $R_{OH}$, $R_{NO_3}$ and $R_{O_3}$, and their corresponding contributions to concentrations, $R_{OH}$, $R_{NO_3}$ and $R_{O_3}$. The order of the major $R_{OH}$, $R_{NO_3}$ and $R_{O_3}$-contributing species differed significantly from that of concentration-contributing species. Therefore, VOC control strategies based on $R_{OH}$, $R_{NO_3}$ and $R_{O_3}$ differ significantly from those based on concentrations.

From the perspective of concentrations, propane, acetone, ethane, n-butane, m/p-xylene, iso-pentane, ethylene, iso-butane, n-pentane and toluene should be targeted. If these 10 species were fully controlled, it would lead to a VOC concentration reduction of 74.1% with only $R_{OH}$, $R_{NO_3}$ and $R_{O_3}$ reductions of 43.1%, 0.4% and 6.4%, respectively. From the perspective of $R_{OH}$, m/p-xylene, ethylene, hexanal, o-xylene, propylene, styrene, methacrolein, cis-butene, methylvinyketone and iso-pentane were the key species. If releases of these compounds were reduced to zero without any offset, it would reduce $R_{OH}$ by 65.1% with a VOC concentration reduction of 24.9%, a $R_{NO_3}$ reduction of 87.1% and a $R_{O_3}$ reduction of 57.1%. From the perspective of $R_{NO_3}$, the top 10 VOC species consisted of styrene, cis-2-butene, trans-2-butene, cis-2-pentene, hexanal, propylene, 1,3-butadiene, 1-butene, trans-2-pentene and pentanal. If the concentrations of these species were completely eliminated, it would reduce $R_{NO_3}$ by 98.0% with a VOC concentration reduction of 4.5%, a $R_{OH}$ reduction of 28.7% and a $R_{O_3}$ reduction of 91.4%. From the perspective of $R_{O_3}$, cis-2-butene, trans-2-butene, propylene, cis-2-pentene, styrene, ethylene, 1-butene, trans-2-pentene, 1-pentene and methacrolein should be key targets for control. If the concentrations of these compounds were reduced to zero without any offset, it would lead to a $R_{O_3}$ reduction of 98.9% with a VOC concentration reduction of 9.1%, a $R_{OH}$ reduction of 31.9% and a $R_{NO_3}$ reduction of 95.6%. Clearly, species with large concentrations do not necessarily have high $R_{OH}$, $R_{NO_3}$ and $R_{O_3}$, and with the least concentration reduction, the maximum reduction of activity can be obtained. The key VOC species of $R_{OH}$, $R_{NO_3}$ and $R_{O_3}$ also differed from each other. However, reducing concentrations of propylene, styrene and cis-butene may likely achieve a win-win-win situation. Although the above comparisons were made under the assumption that concentrations would be significantly reduced, it is obvious that $R_{OH}$, $R_{NO_3}$ and $R_{O_3}$-based control strategies are more efficient than concentration-based policies in terms of reducing VOC pollution.

https://doi.org/10.5194/acp-2019-788
Preprint. Discussion started: 16 December 2019


Atmospheric Chemistry and Physics Discussions

615

616 **3.5 Atmospheric oxidation capacity (AOC)**

617 **3.5.1 Overall characteristics of AOC**

618 The loss rate of VOCs and CO via reactions with OH, $O_3$ and $NO_3$ was calculated. The calculated
619 AOC was up to $4.4\times10^8$ molecules $cm^{-3}$ $s^{-1}$ with campaign-averaged values of $3.1\times10^7$ molecules
620 $cm^{-3}$ $s^{-1}$, daytime averages (06:00-18:00 LT) of $5.2\times10^7$ molecules $cm^{-3}$ $s^{-1}$ and nighttime averages
621 of $1.5\times10^6$ molecules $cm^{-3}$ $s^{-1}$. As such, the total number of CO and VOC molecules depleted during
622 daytime and nighttime were $2.4\times10^{12}$ and $6.1\times10^{10}$, respectively, per $cm^{-3}$ of air. Such AOC levels
623 were lower than those determined at the Tung Chung air quality monitoring station (Xue et al., 2016)
624 and from a polluted area in Santiago, Chile (Elshorbany et al., 2009), but comparable to that
625 determined at the Hong Kong Polytechnic University's air monitoring station at Hok Tsui (Li et al.,
626 2018).

627

628 Comparisons of calculated AOC by OH, $O_3$ and $NO_3$ and corresponding oxidation concentrations
629 are shown in Figure 9. The calculated AOC by OH, $O_3$ and $NO_3$ followed well with the
630 corresponding oxidation concentrations, with correlation coefficients (r) of 0.96, 0.55 and 0.88,
631 respectively, suggesting that the calculated AOC here was consistent with the one obtained using
632 radical concentration to indicate AOC. Specifically, the average oxidation capacities of OH (Figure
633 9a), $O_3$ (Figure 9b) and $NO_3$ (Figure 9c) radicals throughout the entire campaign were $2.9\times10^7$,
634 $1.2\times10^6$ and $1.7\times10^5$ molecule $cm^{-3}$ $s^{-1}$, representing 95.4, 4.0 and 0.6% of the total oxidation
635 capacity, respectively. The total number of depleted molecules per day due to oxidation by OH, $O_3$
636 and $NO_3$ were $2.5\times10^{12}$, $1.1\times10^{11}$ and $1.5\times10^{10}$ molecules $cm^{-3}$, respectively, which was slightly
637 lower than that assessed from a polluted area in Santiago, Chile (Elshorbany et al., 2009).
638 Accordingly, the OH radical is the driving force of the oxidation capacity in the atmosphere in
639 Xianghe, especially during daytime. Figure 10 shows a comparison of the oxidation capacities of
640 OH, $O_3$ and $NO_3$. OH is the only oxidant for CO in the troposphere. As expected, OH was
641 responsible for 97% of the oxidation capacity regarding VOCs and CO during the daytime (Figure
642 10a). The relative contribution of OH initiating oxidation capacity decreased to 94% when
643 restricting the calculation to VOC families alone (Figure 10b). Focusing on the oxidation of
644 unsaturated VOC, OH was the dominant oxidant with a relative proportion of approximately 100%

https://doi.org/10.5194/acp-2019-788
Preprint. Discussion started: 16 December 2019


Atmospheric Chemistry and Physics Discussions

(Figure 10c). Note that the influence of $NO_3$ and $O_3$ on the oxidation of CO and VOCs can be neglected during the daytime. However, the elevated relative contributions of $O_3$ and $NO_3$ initiating oxidation capacity can be observed during nighttime. As expected, $O_3$ and $NO_3$ accounted for 58% and 11%, respectively, of the oxidation capacity regarding VOCs and CO (Figure 10d), but 67% and 13% of VOC families alone (Figure 10e) occurred at night. Focusing on the oxidation of unsaturated VOC, $O_3$ and $NO_3$ accounted for 68% and 13%, respectively, of the oxidation capacity (Figure 10f). Compared with OH and $O_3$, $NO_3$ had a lower contribution during both the daytime and nighttime, which was mainly caused by the high NO concentrations (Liebmann et al., 2018b).

**3.5.2 Relative contributions of VOC oxidation pathways**

VOCs are mainly consumed by reactions with OH radicals, $O_3$ and $NO_3$ radicals in the atmosphere (Tang et al., 2017;Atkinson and Arey, 2003;Yuan et al., 2013;Vereecken and Francisco, 2012). The time series of VOC loss rates due to the reactions with OH radicals, $O_3$ and $NO_3$ radicals are depicted in Figure 11. Diurnal variations of VOC groups and individual species loss rates due to the reactions with different oxidants are shown in Figure 12 and Figure S11-S14, respectively. A comparison of the relative contribution of OH, $NO_3$ and $O_3$ to the daytime and nighttime integral of the oxidation rate is illustrated in Figure 13.

Reactions with OH radicals were the dominant losses for alkanes, accounting for approximately 100% and 99% of the daytime and nighttime average loss rates of alkanes, respectively. In contrast, reactions with $O_3$ and $NO_3$ were nonsignificant for the loss rates of alkanes, accounting for <1% of both the daytime and nighttime average loss rates of alkanes.

Since alkenes have a greater reaction rate with $O_3$, oxidation by $O_3$ also contributes to the loss rates of alkenes. Oxidation by $O_3$ accounted for 24% of the daytime average total loss rate of alkenes and increased to 94% during nighttime. Specifically, the reaction with $O_3$ was the dominant contributor to loss rates of trans-2-butene, cis-2-butene and trans-2-pentene, with daytime contributions of 63, 51 and 56% and nighttime contributions of 91, 87 and 89%, respectively. The relative contributions of $O_3$ to the nighttime integral of the oxidation rates of propylene, 1-butene, 1-pentene and 1-hexene were 61, 54, 72 and 62%, respectively. Reaction oxidation by OH radicals dominated the daytime

https://doi.org/10.5194/acp-2019-788
Preprint. Discussion started: 16 December 2019


Atmospheric Chemistry and Physics Discussions

and nighttime integral of the loss rates of the rest of the species including ethylene, 1,3-butadiene, cis-2-pentene and isoprene. Significantly, in contrast to anthropogenic hydrocarbons, the oxidation by the $NO_3$ radical is more important for the loss rates of isoprene, contributing to <1% and 22% of the daytime and nighttime average loss rates of isoprene, respectively. The contribution of the 24 h average loss rates of isoprene oxidized by $NO_3$ (14%) was much lower than that determined in the Changdao campaign (26%) (Yuan et al., 2013), which was probably caused by the higher $O_3$ concentrations in this study.

For most OVOC species, the reactions with OH radicals were the only significant contributor to OVOC loss rates except for acetone, where the reaction with $O_3$ accounted for 57% of the nighttime average loss rates of acetone. Similar to OVOC species, the reactions with OH radicals were also the only significant contributor to aromatic loss rates, except for styrene, where the reaction with $O_3$ and $NO_3$ accounted for 47% and 46%, respectively, of the nighttime average loss rates of styrene. In total, oxidation by OH radicals accounted for approximately 100% and 81% of the daytime and nighttime average loss rates of OVOCs, respectively. Oxidation by OH radicals, $NO_3$ radicals and $O_3$ accounted for 97, 2 and 1%, respectively, of daytime average loss rates of aromatics, whereas during the nighttime, the contributions from the reactions with OH radicals, $NO_3$ radicals and $O_3$ were 33, 33 and 34%, respectively.

We also emphasized that the concentrations of $NO_3$ are not only influenced by VOCs but also by NO and the heterogeneous loss of $N_2O_5$ (Liebmann et al., 2018b;Yuan et al., 2013;Crowley et al., 2011;Sobanski et al., 2016;Geyer et al., 2001). In this study, $NO_3$ loss due to $N_2O_5$ hydrolysis was not accounted for in Eq. (6). The predicted stationary-state $NO_3$ concentrations calculated from Eq. (6) were upper limits, and hence, the calculation of $NO_3$ contributions to VOC losses was also overestimated.

## 4 Conclusions

In the summer of 2018, a comprehensive field campaign was conducted at a suburban site in the North China Plain. Based on simultaneous measurements of $O_3$, CO, $SO_2$, NO, $NO_2$, $J_{O^1D}$, $J_{NO_2}$, $J_{NO_3}$ and 65 VOCs, reactivities (OH, $NO_3$ and $O_3$ reactivities) for trace gases and atmospheric

https://doi.org/10.5194/acp-2019-788
Preprint. Discussion started: 16 December 2019


Atmospheric Chemistry and Physics Discussions

oxidation capacity (AOC) were comprehensively analyzed. The main findings are summarized as follows.

The total, $R_{OH}^{\text{total}}$, was between 8.5 and 68.1 $s^{-1}$ with an average of 25.6±9.7 $s^{-1}$, which was mainly contributed by $NO_x$ (12.0±7.1 $s^{-1}$, 47%), followed by CO (7.2±2.6 $s^{-1}$, 28%) and TVOCs (6.2±4.6 $s^{-1}$, 24%) and to a lesser extent by $SO_2$ and $O_3$ (0.2±0.1 $s^{-1}$, 1%). $R_{OH}^{\text{TVOCs}}$ was 6.2±4.6 $s^{-1}$ and dominated by isoprene. Campaign-averaged values of $R_{NO_3}^{\text{total}}$ were 2.2±2.6 $s^{-1}$, ranging from 0.7 $s^{-1}$ to 27.5 $s^{-1}$. $NO_x$ was by far the main contributors to the $R_{NO_3}^{\text{total}}$, representing 99% of the $R_{NO_3}^{\text{total}}$ on average. $R_{NO_3}^{\text{TVOCs}}$ was 2.2±2.7×$10^{-2}$ $s^{-1}$ on average with a minimum of 1.0×$10^{-3}$ $s^{-1}$ and a maximum of 0.2 $s^{-1}$. The largest fraction of attributed $R_{NO_3}^{\text{TVOCs}}$ was contributed by isoprene (77%). The $R_{O_3}^{\text{total}}$ varied between a minimum of 3.3×$10^{-4}$ $s^{-1}$ and a maximum of 1.8×$10^{-2}$ $s^{-1}$ and was 1.2±1.7×$10^{-3}$ $s^{-1}$ on average. NO exhibited the most prominent contribution to the $R_{O_3}^{\text{total}}$ and represented an average of >99% of the $R_{O_3}^{\text{total}}$. $R_{O_3}^{\text{TVOCs}}$ was 1.1±0.8×$10^{-6}$ $s^{-1}$ on average, ranging from 2.5×$10^{-7}$ $s^{-1}$ to 1.0×$10^{-5}$ $s^{-1}$. Alkenes clearly dominated the $R_{O_3}^{\text{TVOCs}}$ with campaign-averaged contributions of 66%.

$R_{OH}^{\text{total}}$, $R_{NO_3}^{\text{total}}$ and $R_{O_3}^{\text{total}}$ displayed a similar diel variation with the lowest in the afternoon and the highest during rush hours, and the diurnal profile of $NO_x$ appears to be the major driver for the diurnal profiles of $R_{OH}^{\text{total}}$, $R_{NO_3}^{\text{total}}$ and $R_{O_3}^{\text{total}}$. Compared with $R_{OH}$ and $R_{NO_3}$, $R_{O_3}$ displayed a much weaker diel variation, especially $R_{O_3}^{\text{alkenes}}$ and $R_{O_3}^{\text{aromatics}}$ due to 1) the rate coefficients with $O_3$ being much smaller than the corresponding reaction rate coefficients with OH and $NO_3$ for the same species and 2) the high-emissions species reaction rate coefficients with $O_3$ being smaller than the low-emissions species reaction rate coefficients with $O_3$.

The $R_{OH}^{\text{VOCs}}/R_{OH}^{\text{NO}_x}$ ratio and scatter plots of CO-$NO_y$ color-coded with $O_3$ concentrations indicated a VOC-limited regime of $O_3$ formation in Xianghe, suggesting that control of VOCs would be most effective for controlling $O_3$ in Xianghe. $R_{OH}$, $R_{NO_3}$ and $R_{O_3}$-based control strategies are more efficient than concentration-based policies in terms of reducing VOC pollution. We suggest that policy makers shift the current concentration -based limits to reactivity-based policies.

https://doi.org/10.5194/acp-2019-788
Preprint. Discussion started: 16 December 2019


Atmospheric Chemistry and Physics Discussions

735 The loss rates of VOCs and CO via reactions with OH, $O_3$ and $NO_3$ were calculated, which were up
736 to $4.4\times10^8$ molecules $cm^{-3}$ $s^{-1}$ with campaign-averaged values of $3.1\times10^7$ molecules $cm^{-3}$ $s^{-1}$,
737 daytime averages (06:00-18:00 LT) of $5.2\times10^7$ molecules $cm^{-3}$ $s^{-1}$ and nighttime averages of
738 $1.5\times10^6$ molecules $cm^{-3}$ $s^{-1}$. The AOC was dominated by OH radicals ($2.9\times10^7$ molecule $cm^{-3}$ $s^{-1}$,
739 95%), $O_3$ ($1.2\times10^6$ molecule $cm^{-3}$ $s^{-1}$, 4%) and $NO_3$ radicals ($1.7\times10^5$ molecule $cm^{-3}$ $s^{-1}$, 1%),
740 suggesting that the OH radical is the driving force of the oxidation capacity in the atmosphere in
741 Xianghe, especially during the daytime. The reaction with OH radicals was the dominant loss for
742 VOCs except for trans-2-butene, cis-2-butene, trans-2-pentene, propylene, 1-butene, 1-pentene, 1-
743 hexene, acetone and styrene, where the reaction with $O_3$ was more important for their loss rates.
744 Compared with anthropogenic hydrocarbons, the oxidation by $NO_3$ radical was more important for
745 the nighttime integral of isoprene loss rates.
746
747 Our study provides useful insights for VOC pollution control in a typical suburban site in the North
748 China Plain. Further studies, especially direct observations of the OH and $NO_3$ radical, OH and $NO_3$
749 reactivity measurements and speciated measurements, are required to further explore the trace gas
750 reactivity and AOC.
751

752 **Acknowledgement**

753 This study was financially supported by the Ministry of Science and Technology of China
754 (2017YFC0210000), Beijing Major Science and Technology Project (Z181100005418014). All
755 referenced supplemental figures and tables can be found in the supporting information. The authors
756 are grateful to all staff and workers from the Xianghe Atmospheric Observatory of Institute of
757 Atmospheric Physics (IAP) of the Chinese Academy of Sciences for their support during the
758 sampling campaign. We also acknowledge National Meteorological Information Center for
759 providing high quality meteorology parameters.
760

761 **Competing financial interests**

762 The authors declare no competing financial interests.
763

https://doi.org/10.5194/acp-2019-788
Preprint. Discussion started: 16 December 2019


Atmospheric Chemistry and Physics Discussions

764 **Author contributions**

765 Y.S.W designed the research. Y.Y and D.Y, S.M.Z, D.S.J, Y.H.W conducted the measurements. Y.Y
766 and Y.H.W interpreted the data and write the paper. All the authors commented on the paper.

767

768

769 **Reference**

770 Alicke, B.: Impact of nitrous acid photolysis on the total hydroxyl radical budget during the
771 Limitation of Oxidant Production/Pianura Padana Produzione di Ozono study in Milan, Journal of
772 Geophysical Research, 107, doi:10.1029/2000jd000075, 2002.
773 Asaf, D., Pedersen, D., Matveev, V., Peleg, M., Kern, C., Zingler, J., Platt, U., and Luria, M.: Long-
774 Term Measurements of $NO_3$ Radical at a Semiarid Urban Site: 1. Extreme Concentration Events
775 and Their Oxidation Capacity, Environ Sci Technol, 43, 9117-9123, doi:10.1021/es900798b, 2009.
776 Atkinson, R., Winer, A. M., and Pitts, J. N.: Estimation of night-time $N_2O_5$ concentrations from
777 ambient $NO_2$ and $NO_3$ radical concentrations and the role of $N_2O_5$ in night-time chemistry, Atmos
778 Environ, 20, 331-339, https://doi.org/10.1016/0004-6981(86)90035-1, 1986.
779 Atkinson, R.: Atmospheric chemistry of VOCs and NOx, Atmos Environ, 34, 2063-2101,
780 doi:10.1016/S1352-2310(99)00460-4, 2000.
781 Atkinson, R., and Arey, J.: Atmospheric Degradation of Volatile Organic Compounds., Chemical
782 Reviews, 103, 4605-4638, doi:10.102/cr0206420, 2003.
783 Atkinson, R., Baulch, D. L., Cox, R. A., Crowley, J. N., Hampson, R. F., Hynes, R. G., Jenkin, M.
784 E., Rossi, M. J., and Troe, J.: Evaluated kinetic and photochemical data for atmospheric chemistry:
785 Volume I - gas phase reactions of Ox, HOx, NOx and SOx species, Atmos. Chem. Phys., 4, 1461-
786 1738, doi:10.5194/acp-4-1461-2004, 2004.
787 Atkinson, R., Baulch, D. L., Cox, R. A., Crowley, J. N., Hampson, R. F., Hynes, R. G., Jenkin, M.
788 E., Rossi, M. J., and Troe, J.: Evaluated kinetic and photochemical data for atmospheric chemistry:
789 Volume II – gas phase reactions of organic species, Atmos Chem Phys, 6, 3625-4055,
790 doi:10.5194/acp-6-3625-2006, 2006a.
791 Atkinson, R., Baulch, D. L., Cox, R. A., Crowley, J. N., Hampson, R. F., Hynes, R. G., Jenkin, M.
792 E., Rossi, M. J., Troe, J., and Subcommittee, I.: Evaluated kinetic and photochemical data for
793 atmospheric chemistry: Volume II - gas phase reactions of organic species, Atmos. Chem. Phys., 6,

https://doi.org/10.5194/acp-2019-788
Preprint. Discussion started: 16 December 2019




794 3625-4055, doi:10.5194/acp-6-3625-2006, 2006b.
795 Benedict, K. B., Zhou, Y., Sive, B. C., Prenni, A. J., Gebhart, K. A., Fischer, E. V., Evanoski-Cole,
796 A., Sullivan, A. P., Callahan, S., Schichtel, B. A., Mao, H., Zhou, Y., and Collett Jr, J. L.: Volatile
797 Organic Compounds and Ozone in Rocky Mountain National Park during FRAPPÉ, Atmos Chem
798 Phys, 19, 499-521, doi:10.5194/acp-19-499-2019, 2019.
799 Bsaibes, S., Al Ajami, M., Mermet, K., Truong, F., Batut, S., Hecquet, C., Dusanter, S., Léornadis,
800 T., Sauvage, S., Kammer, J., Flaud, P.-M., Perraudin, E., Villenave, E., Locoge, N., Gros, V., and
801 Schoemaecker, C.: Variability of OH reactivity in the Landes maritime Pine forest: Results from the
802 LANDEX campaign 2017, Atmospheric Chemistry and Physics Discussions, 1-35,
803 doi:10.5194/acp-2019-548, 2019.
804 Carter, W. P. L.: Development of Ozone Reactivity Scales for Volatile Organic Compounds, Air &
805 Waste, 44, 881-899, doi:10.1080/1073161x.1994.10467290, 2012.
806 Chen, W. T., Shao, M., Lu, S. H., Wang, M., Zeng, L. M., Yuan, B., and Liu, Y.: Understanding
807 primary and secondary sources of ambient carbonyl compounds in Beijing using the PMF model,
808 Atmos Chem Phys, 14, 3047-3062, doi:10.5194/acp-14-3047-2014, 2014.
809 Chen, X., Millet, D. B., Singh, H. B., Wisthaler, A., Apel, E. C., Atlas, E. L., Blake, D. R., Brown,
810 S. S., Crounse, J. D., de Gouw, J. A., Flocke, F., Fried, A., Heikes, B. G., Hornbrook, R. S., Mikoviny,
811 T., Min, K.-E., Müller, M., Neuman, J. A., amp, apos, Sullivan, D. W., Peischl, J., Pfister, G. G.,
812 Richter, D., Roberts, J. M., Ryerson, T. B., Shertz, S., Treadaway, V., Veres, P. R., Walega, J.,
813 Warneke, C., Washenfelder, R. A., Weibring, P., and Yuan, B.: On the sources and sinks of
814 atmospheric VOCs: An integrated analysis of recent aircraft campaigns over North America, Atmos
815 Chem Phys, 19, 9097-9123, doi:10.5194/acp-19-9097-2019, 2019.
816 Crowley, J. N., Thieser, J., Tang, M. J., Schuster, G., Bozem, H., Beygi, Z. H., Fischer, H., Diesch,
817 J. M., Drewnick, F., Borrmann, S., Song, W., Yassaa, N., Williams, J., Pöhler, D., Platt, U., and
818 Lelieveld, J.: Variable lifetimes and loss mechanisms for $NO_3$ and $N_2O_5$ during the DOMINO
819 campaign: contrasts between marine, urban and continental air, Atmos Chem Phys, 11, 10853-10870,
820 doi:10.5194/acp-11-10853-2011, 2011.
821 de Gouw, J. A., Warneke, C., Stohl, A., Wollny, A. G., Brock, C. A., Cooper, O. R., Holloway, J. S.,
822 Trainer, M., Fehsenfeld, F. C., Atlas, E. L., Donnelly, S. G., Stroud, V., and Lueb, A.: Volatile organic
823 compounds composition of merged and aged forest fire plumes from Alaska and western Canada,

https://doi.org/10.5194/acp-2019-788
Preprint. Discussion started: 16 December 2019




824 Journal of Geophysical Research: Atmospheres, 111, D10303, doi:10.1029/2005jd006175, 2006.
825 Derwent, R. G., Middleton, D. R., Field, R. A., Goldstone, M. E., Lester, J. N., and Perry, R.:
826 Analysis and interpretation of air quality data from an urban roadside location in Central London
827 over the period from July 1991 to July 1992, Atmos Environ, 28, 923-946, doi:10.1016/1352-
828 2310(94)00219-B, 1995.
829 Di Carlo, P., Brune, W. H., Martinez, M., Harder, H., Lesher, R., Ren, X., Thornberry, T., Carroll,
830 M. A., Young, V., Shepson, P. B., Riemer, D., Apel, E., and Campbell, C.: Missing OH reactivity in
831 a forest: evidence for unknown reactive biogenic VOCs, Science, 304, 722-725,
832 doi:10.1126/science.1094392, 2004.
833 Ding, A. J., Fu, C. B., Yang, X. Q., Sun, J. N., Zheng, L. F., Xie, Y. N., Herrmann, E., Nie, W., Petäjä,
834 T., Kerminen, V. M., and Kulmala, M.: Ozone and fine particle in the western Yangtze River Delta:
835 an overview of 1 yr data at the SORPES station, Atmos Chem Phys, 13, 5813-5830,
836 doi:10.5194/acp-13-5813-2013, 2013.
837 Ding, X., He, Q.-F., Shen, R.-Q., Yu, Q.-Q., and Wang, X.-M.: Spatial distributions of secondary
838 organic aerosols from isoprene, monoterpenes, β-caryophyllene, and aromatics over China during
839 summer, Journal of Geophysical Research: Atmospheres, 119, 11,877-811,891,
840 doi:10.1002/2014jd021748, 2014.
841 Dolgorouky, C., Gros, V., Sarda-Esteve, R., Sinha, V., Williams, J., Marchand, N., Sauvage, S.,
842 Poulain, L., Sciare, J., and Bonsang, B.: Total OH reactivity measurements in Paris during the 2010
843 MEGAPOLI winter campaign, Atmos Chem Phys, 12, 9593-9612, doi:10.5194/acp-12-9593-2012,
844 2012.
845 Edwards, P. M., Evans, M. J., Furneaux, K. L., Hopkins, J., Ingham, T., Jones, C., Lee, J. D., Lewis,
846 A. C., Moller, S. J., Stone, D., Whalley, L. K., and Heard, D. E.: OH reactivity in a South East Asian
847 tropical rainforest during the Oxidant and Particle Photochemical Processes (OP3) project, Atmos
848 Chem Phys, 13, 9497-9514, doi:10.5194/acp-13-9497-2013, 2013.
849 Ehhalt, D. H., and Rohrer, F.: Dependence of the OH concentration on solar UV, Journal of
850 Geophysical Research, 105, 3565-3571, doi:10.1029/1999jd901070, 2000.
851 Elshorbany, Y. F., Kurtenbach, R., Wiesen, P., Lissi, E., Rubio, M., Villena, G., Gramsch, E., Rickard,
852 A. R., Pilling, M. J., and Kleffmann, J.: Oxidation capacity of the city air of Santiago, Chile, Atmos
853 Chem Phys, 9, 2257-2273, doi:10.5194/acp-9-2257-2009, 2009.

https://doi.org/10.5194/acp-2019-788
Preprint. Discussion started: 16 December 2019


Atmospheric Chemistry and Physics Discussions

854 Elshorbany, Y. F., Kleffmann, J., Hofzumahaus, A., Kurtenbach, R., Wiesen, P., Brauers, T., Bohn,
855 B., Dorn, H. P., Fuchs, H., Holland, F., Rohrer, F., Tillmann, R., Wegener, R., Wahner, A., Kanaya,
856 Y., Yoshino, A., Nishida, S., Kajii, Y., Martinez, M., Kubistin, D., Harder, H., Lelieveld, J., Elste, T.,
857 Plass-Dülmer, C., Stange, G., Berresheim, H., and Schurath, U.: HOx budgets during HOxComp: A
858 case study of HOx chemistry under NOx-limited conditions, Journal of Geophysical Research:
859 Atmospheres, 117, doi:10.1029/2011jd017008, 2012.
860 Ferracci, V., Heimann, I., Abraham, N. L., Pyle, J. A., and Archibald, A. T.: Global modelling of the
861 total OH reactivity: investigations on the "missing" OH sink and its atmospheric implications,
862 Atmos Chem Phys, 18, 7109-7129, doi:10.5194/acp-18-7109-2018, 2018.
863 Fuchs, H., Novelli, A., Rolletter, M., Hofzumahaus, A., Pfannerstill, E. Y., Kessel, S., Edtbauer, A.,
864 Williams, J., Michoud, V., Dusanter, S., Locoge, N., Zannoni, N., Gros, V., Truong, F., Sarda-Esteve,
865 R., Cryer, D. R., Brumby, C. A., Whalley, L. K., Stone, D., Seakins, P. W., Heard, D. E.,
866 Schoemaecker, C., Blocquet, M., Coudert, S., Batut, S., Fittschen, C., Thames, A. B., Brune, W. H.,
867 Ernest, C., Harder, H., Muller, J. B. A., Elste, T., Kubistin, D., Andres, S., Bohn, B., Hohaus, T.,
868 Holland, F., Li, X., Rohrer, F., Kiendler-Scharr, A., Tillmann, R., Wegener, R., Yu, Z., Zou, Q., and
869 Wahner, A.: Comparison of OH reactivity measurements in the atmospheric simulation chamber
870 SAPHIR, Atmos Meas Tech, 10, 4023-4053, doi:10.5194/amt-10-4023-2017, 2017a.
871 Fuchs, H., Tan, Z., Lu, K., Bohn, B., Broch, S., Brown, S. S., Dong, H., Gomm, S., Häseler, R., He,
872 L., Hofzumahaus, A., Holland, F., Li, X., Liu, Y., Lu, S., Min, K.-E., Rohrer, F., Shao, M., Wang,
873 B., Wang, M., Wu, Y., Zeng, L., Zhang, Y., Wahner, A., and Zhang, Y.: OH reactivity at a rural site
874 (Wangdu) in the North China Plain: contributions from OH reactants and experimental OH budget,
875 Atmos Chem Phys, 17, 645-661, doi:10.5194/acp-17-645-2017, 2017b.
876 Gerasopoulos, E., Kazadzis, S., Vrekoussis, M., Kouvarakis, G., Liakakou, E., Kouremeti, N.,
877 Giannadaki, D., Kanakidou, M., Bohn, B., and Mihalopoulos, N.: Factors affecting O3 and NO2
878 photolysis frequencies measured in the eastern Mediterranean during the five-year period 2002-
879 2006, Journal of Geophysical Research: Atmospheres, 117, doi:10.1029/2012jd017622, 2012.
880 Geyer, A., Alicke, B., Konrad, S., Schmitz, T., Stutz, J., and Platt, U.: Chemistry and oxidation
881 capacity of the nitrate radical in the continental boundary layer near Berlin, Journal of Geophysical
882 Research: Atmospheres, 106, 8013-8025, doi:10.1029/2000jd900681, 2001.
883 Geyer, A.: Nighttime formation of peroxy and hydroxyl radicals during the BERLIOZ campaign:

https://doi.org/10.5194/acp-2019-788
Preprint. Discussion started: 16 December 2019




884 Observations and modeling studies, Journal of Geophysical Research, 108,
885 doi:10.1029/2001jd000656, 2003.
886 Goldan, P. D., Kuster, W. C., Williams, E., Murphy, P. C., Fehsenfeld, F. C., and Meagher, J.:
887 Nonmethane hydrocarbon and oxy hydrocarbon measurements during the 2002 New England Air
888 Quality Study, Journal of Geophysical Research: Atmospheres, 109, D21309,
889 doi:10.1029/2003jd004455, 2004.
890 Goldstein, A. H., and Galbally, I. E.: Known and unexplored organic constituents in the earth's
891 atmosphere, Environ Sci Technol, 41, 1514-1521, doi:10.1021/es072476p, 2007.
892 Guenther, A., Hewitt, C. N., Erickson, D., Fall, R., Geron, C., Graedel, T., Harley, P., Klinger, L.,
893 Lerdau, M., McKay, W. A., Pierce, T., Scholes, B., Steinbrecher, R., Tallamraju, R., Taylor, J., and
894 Zimmerman, P.: A global model of natural volatile organic compound emissions, Journal of
895 Geophysical Research, 100, 8873, doi:10.1029/94jd02950, 1995.
896 Guenther, A. B., Zimmerman, P. R., Harley, P. C., Monson, R. K., and Fall, R.: Isoprene and
897 monoterpene emission rate variability: Model evaluations and sensitivity analyses, Journal of
898 Geophysical Research, 98, 12609-12617, doi:10.1029/93JD00527, 1993.
899 He, Z., Wang, X., Ling, Z., Zhao, J., Guo, H., Shao, M., and Wang, Z.: Contributions of different
900 anthropogenic volatile organic compound sources to ozone formation at a receptor site in the Pearl
901 River Delta region and its policy implications, Atmospheric Chemistry and Physics Discussions, 1-
902 34, doi:10.5194/acp-2018-1293, 2019.
903 Heard, D. E., and Pilling, M. J.: Measurement of OH and HO2 in the troposphere, Chemical Reviews,
904 103, 5163-5198, doi:10.1021/cr020522s, 2003.
905 Jenkin, M. E., Young, J. C., and Rickard, A. R.: The MCM v3.3.1 degradation scheme for isoprene,
906 Atmos Chem Phys, 15, 11433-11459, doi:10.5194/acp-15-11433-2015, 2015.
907 Kaiser, J., Skog, K. M., Baumann, K., Bertman, S. B., Brown, S. B., Brune, W. H., Crounse, J. D.,
908 de Gouw, J. A., Edgerton, E. S., Feiner, P. A., Goldstein, A. H., Koss, A., Misztal, P. K., Nguyen, T.
909 B., Olson, K. F., St. Clair, J. M., Teng, A. P., Toma, S., Wennberg, P. O., Wild, R. J., Zhang, L., and
910 Keutsch, F. N.: Speciation of OH reactivity above the canopy of an isoprene-dominated forest,
911 Atmos Chem Phys, 16, 9349-9359, doi:10.5194/acp-16-9349-2016, 2016.
912 Kansal, A.: Sources and reactivity of NMHCs and VOCs in the atmosphere: a review, J Hazard
913 Mater, 166, 17-26, doi:10.1016/j.jhazmat.2008.11.048, 2009.

https://doi.org/10.5194/acp-2019-788
Preprint. Discussion started: 16 December 2019




914 Kirchner, F., Jeanneret, F., Clappier, A., Krüger, B., van den Bergh, H., and Calpini, B.: Total VOC
915 reactivity in the planetary boundary layer: 2. A new indicator for determining the sensitivity of the
916 ozone production to VOC and NOx, Journal of Geophysical Research: Atmospheres, 106, 3095-
917 3110, doi:10.1029/2000jd900603, 2001.
918 Kovacs, T. A., Brune, W. H., Harder, H., Martinez, M., Simpas, J. B., Frost, G. J., Williams, E.,
919 Jobson, T., Stroud, C., Young, V., Fried, A., and Wert, B.: Direct measurements of urban OH
920 reactivity during Nashville SOS in summer 1999, J Environ Monitor, 5, 68-74,
921 doi:10.1039/b204339d, 2003.
922 Lee, J. D., Young, J. C., Read, K. A., Hamilton, J. F., Hopkins, J. R., Lewis, A. C., Bandy, B. J.,
923 Davey, J., Edwards, P., Ingham, T., Self, D. E., Smith, S. C., Pilling, M. J., and Heard, D. E.:
924 Measurement and calculation of OH reactivity at a United Kingdom coastal site, J Atmos Chem, 64,
925 53-76, doi:10.1007/s10874-010-9171-0, 2010.
926 Leuchner, M., and Rappenglück, B.: VOC source–receptor relationships in Houston during
927 TexAQS-II, Atmos Environ, 44, 4056-4067, doi:10.1016/j.atmosenv.2009.02.029, 2010.
928 Li, K., Jacob, D. J., Liao, H., Shen, L., Zhang, Q., and Bates, K. H.: Anthropogenic drivers of 2013-
929 2017 trends in summer surface ozone in China, Proc Natl Acad Sci U S A, 116, 422-427,
930 doi:10.1073/pnas.1812168116, 2019a.
931 Li, M., Zhang, Q., Zheng, B., Tong, D., Lei, Y., Liu, F., Hong, C., Kang, S., Yan, L., Zhang, Y., Bo,
932 Y., Su, H., Cheng, Y., and He, K.: Persistent growth of anthropogenic non-methane volatile organic
933 compound (NMVOC) emissions in China during 1990–2017: drivers, speciation and ozone
934 formation potential, Atmos Chem Phys, 19, 8897-8913, doi:10.5194/acp-19-8897-2019, 2019b.
935 Li, Z., Xue, L., Yang, X., Zha, Q., Tham, Y. J., Yan, C., Louie, P. K. K., Luk, C. W. Y., Wang, T.,
936 and Wang, W.: Oxidizing capacity of the rural atmosphere in Hong Kong, Southern China, Sci Total
937 Environ, 612, 1114-1122, doi:10.1016/j.scitotenv.2017.08.310, 2018.
938 Liebmann, J., Karu, E., Sobanski, N., Schuladen, J., Ehn, M., Schallhart, S., Quéléver, L., Hellen,
939 H., Hakola, H., Hoffmann, T., Williams, J., Fischer, H., Lelieveld, J., and Crowley, J. N.: Direct
940 measurement of $NO_3$ radical reactivity in a boreal forest, Atmos Chem Phys, 18, 3799-3815,
941 doi:10.5194/acp-18-3799-2018, 2018a.
942 Liebmann, J. M., Schuster, G., Schuladen, J. B., Sobanski, N., Lelieveld, J., and Crowley, J. N.:
943 Measurement of ambient NO3 reactivity: design, characterization and first deployment of a new

https://doi.org/10.5194/acp-2019-788
Preprint. Discussion started: 16 December 2019




944 instrument, Atmos Meas Tech, 10, 1241-1258, doi:10.5194/amt-10-1241-2017, 2017.
945 Liebmann, J. M., Muller, J. B. A., Kubistin, D., Claude, A., Holla, R., Plass-Dülmer, C., Lelieveld,
946 J., and Crowley, J. N.: Direct measurements of $NO_3$ reactivity in and above the boundary layer of a
947 mountaintop site: identification of reactive trace gases and comparison with OH reactivity, Atmos
948 Chem Phys, 18, 12045-12059, doi:10.5194/acp-18-12045-2018, 2018b.
949 Liu, Y., Shao, M., Lu, S. H., Liao, C. C., Wang, J. L., and Chen, G.: Volatile organic compound
950 (VOC) measurements in the pearl river delta (PRD) region, China, Atmos Chem Phys, 8, 1531-1545,
951 doi:10.5194/acp-8-1531-2008, 2008.
952 Lou, S., Holland, F., Rohrer, F., Lu, K., Bohn, B., Brauers, T., Chang, C. C., Fuchs, H., Häseler, R.,
953 Kita, K., Kondo, Y., Li, X., Shao, M., Zeng, L., Wahner, A., Zhang, Y., Wang, W., and Hofzumahaus,
954 A.: Atmospheric OH reactivities in the Pearl River Delta – China in summer 2006: measurement
955 and model results, Atmos Chem Phys, 10, 11243-11260, doi:10.5194/acp-10-11243-2010, 2010.
956 Lu, K., Zhang, Y., Su, H., Brauers, T., Chou, C. C., Hofzumahaus, A., Liu, S. C., Kita, K., Kondo,
957 Y., Shao, M., Wahner, A., Wang, J., Wang, X., and Zhu, T.: Oxidant ($O_3$+ $NO_2$) production processes
958 and formation regimes in Beijing, Journal of Geophysical Research, 115,
959 doi:10.1029/2009jd012714, 2010.
960 Lyu, X., Wang, N., Guo, H., Xue, L., Jiang, F., Zeren, Y., Cheng, H., Cai, Z., Han, L., and Zhou, Y.:
961 Causes of a continuous summertime O3 pollution event in Jinan, a central city in the North China
962 Plain, Atmos Chem Phys, 19, 3025-3042, doi:10.5194/acp-19-3025-2019, 2019.
963 Mao, J., Ren, X., Brune, W. H., Olson, J. R., Crawford, J. H., Fried, A., Huey, L. G., Cohen, R. C.,
964 Heikes, B., Singh, H. B., Blake, D. R., Sachse, G. W., Diskin, G. S., Hall, S. R., and Shetter, R. E.:
965 Airborne measurement of OH reactivity during INTEX-B, Atmos. Chem. Phys., 9, 163-173,
966 doi:10.5194/acp-9-163-2009, 2009.
967 Mao, J., Ren, X., Chen, S., Brune, W. H., Chen, Z., Martinez, M., Harder, H., Lefer, B., Rappenglück,
968 B., Flynn, J., and Leuchner, M.: Atmospheric oxidation capacity in the summer of Houston 2006:
969 Comparison with summer measurements in other metropolitan studies, Atmos Environ, 44, 4107-
970 4115, doi:10.1016/j.atmosenv.2009.01.013, 2010.
971 Pacifico, F., Harrison, S. P., Jones, C. D., and Sitch, S.: Isoprene emissions and climate, Atmos
972 Environ, 43, 6121-6135, doi:10.1016/j.atmosenv.2009.09.002, 2009.
973 Pfannerstill, E. Y., Wang, N. J., Edtbauer, A., Bourtsoukidis, E., Crowley, J. N., Dienhart, D., Eger,

https://doi.org/10.5194/acp-2019-788
Preprint. Discussion started: 16 December 2019


Atmospheric Chemistry and Physics Discussions

974 P. G., Ernle, L., Fischer, H., Hottmann, B., Paris, J. D., Stonner, C., Tadic, I., Walter, D., and
975 Williams, J.: Shipborne measurements of total OH reactivity around the Arabian Peninsula and its
976 role in ozone chemistry, Atmos Chem Phys, 19, 11501-11523, doi:10.5194/acp-19-11501-2019,
977 2019.
978 Piccot, S. D., Watson, J. J., and Jones, J. W.: A global inventory of volatile organic compound
979 emissions from anthropogenic sources, Journal of Geophysical Research: Atmospheres, 97, 9897-
980 9912, doi:10.1029/92jd00682, 1992.
981 Pusede, S. E., and Cohen, R. C.: On the observed response of ozone to NOx and VOC reactivity
982 reductions in San Joaquin Valley California 1995–present, Atmos Chem Phys, 12, 8323-8339,
983 doi:10.5194/acp-12-8323-2012, 2012.
984 Ramasamy, S., Ida, A., Jones, C., Kato, S., Tsurumaru, H., Kishimoto, I., Kawasaki, S., Sadanaga,
985 Y., Nakashima, Y., Nakayama, T., Matsumi, Y., Mochida, M., Kagami, S., Deng, Y., Ogawa, S.,
986 Kawana, K., and Kajii, Y.: Total OH reactivity measurement in a BVOC dominated temperate forest
987 during a summer campaign, 2014, Atmos Environ, 131, 41-54, doi:10.1016/j.atmosenv.2016.01.039,
988 2016.
989 Ren, X.: HOx concentrations and OH reactivity observations in New York City during PMTACS-
990 NY2001, Atmos Environ, 37, 3627-3637, doi:10.1016/s1352-2310(03)00460-6, 2003.
991 Ren, X., Brune, W. H., Mao, J., Mitchell, M. J., Lesher, R. L., Simpas, J. B., Metcalf, A. R., Schwab,
992 J. J., Cai, C., and Li, Y.: Behavior of OH and $HO_2$ in the winter atmosphere in New York City, Atmos
993 Environ, 40, 252-263, doi:10.1016/j.atmosenv.2005.11.073, 2006a.
994 Ren, X., Brune, W. H., Oliger, A., Metcalf, A. R., Simpas, J. B., Shirley, T., Schwab, J. J., Bai, C.,
995 Roychowdhury, U., Li, Y., Cai, C., Demerjian, K. L., He, Y., Zhou, X., Gao, H., and Hou, J.: OH,
996 $HO_2$, and OH reactivity during the PMTACS-NY Whiteface Mountain 2002 campaign:
997 Observations and model comparison, Journal of Geophysical Research: Atmospheres, 111,
998 doi:10.1029/2005jd006126, 2006b.
999 Sadanaga, Y., Yoshino, A., Kato, S., and Kajii, Y.: Measurements of OH reactivity and
1000 photochemical ozone production in the urban atmosphere, Environ Sci Technol, 39, 8847-8852,
1001 doi:10.1021/es049457p, 2005.
1002 Saunier, A., Ormeño, E., Boissard, C., Wortham, H., Temime-Roussel, B., Lecareux, C., Armengaud,
1003 A., and Fernandez, C.: Effect of mid-term drought on Quercus pubescens BVOCs' emission

https://doi.org/10.5194/acp-2019-788
Preprint. Discussion started: 16 December 2019




1004 seasonality and their dependency on light and/or temperature, Atmos Chem Phys, 17, 7555-7566,
1005 doi:10.5194/acp-17-7555-2017, 2017.
1006 Shirley, T. R., Brune, W. H., Ren, X., Mao, J., Lesher, R., Cardenas, B., Volkamer, R., Molina, L. T.,
1007 Molina, M. J., Lamb, B., Velasco, E., Jobson, T., and Alexander, M.: Atmospheric oxidation in the
1008 Mexico City Metropolitan Area (MCMA) during April 2003, Atmos Chem Phys, 6, 2753-2765,
1009 doi:10.5194/acp-6-2753-2006, 2006.
1010 Sinha, V., Williams, J., Crowley, J. N., and Lelieveld, J.: The Comparative Reactivity Method
1011 – a new tool to measure total OH Reactivity in ambient air, Atmos. Chem. Phys., 8, 2213-
1012 2227, doi:10.5194/acp-8-2213-2008, 2008.
1013 Sinha, V., Williams, J., Diesch, J. M., Drewnick, F., Martinez, M., Harder, H., Regelin, E., Kubistin,
1014 D., Bozem, H., Hosaynali-Beygi, Z., Fischer, H., Andrés-Hernández, M. D., Kartal, D., Adame, J.
1015 A., and Lelieveld, J.: Constraints on instantaneous ozone production rates and regimes during
1016 DOMINO derived using in-situ OH reactivity measurements, Atmos Chem Phys, 12, 7269-7283,
1017 doi:10.5194/acp-12-7269-2012, 2012.
1018 Sobanski, N., Tang, M. J., Thieser, J., Schuster, G., Pöhler, D., Fischer, H., Song, W., Sauvage, C.,
1019 Williams, J., Fachinger, J., Berkes, F., Hoor, P., Platt, U., Lelieveld, J., and Crowley, J. N.: Chemical
1020 and meteorological influences on the lifetime of $NO_3$ at a semi-rural mountain site during PARADE,
1021 Atmos Chem Phys, 16, 4867-4883, doi:10.5194/acp-16-4867-2016, 2016.
1022 Sonderfeld, H., White, I. R., Goodall, I. C. A., Hopkins, J. R., Lewis, A. C., Koppmann, R., and
1023 Monks, P. S.: What effect does VOC sampling time have on derived OH reactivity?, Atmos Chem
1024 Phys, 16, 6303-6318, doi:10.5194/acp-16-6303-2016, 2016.
1025 Song, M. D., Tan, Q. W., Feng, M., Qu, Y., Liu, X. G., An, J. L., and Zhang, Y. H.: Source
1026 Apportionment and Secondary Transformation of Atmospheric Nonmethane Hydrocarbons in
1027 Chengdu, Southwest China, J Geophys Res-Atmos, 123, 9741-9763, doi:10.1029/2018jd028479,
1028 2018.
1029 Tan, Z., Lu, K., Jiang, M., Su, R., Wang, H., Lou, S., Fu, Q., Zhai, C., Tan, Q., Yue, D., Chen, D.,
1030 Wang, Z., Xie, S., Zeng, L., and Zhang, Y.: Daytime atmospheric oxidation capacity in four Chinese
1031 megacities during the photochemically polluted season: a case study based on box model simulation,
1032 Atmos Chem Phys, 19, 3493-3513, doi:10.5194/acp-19-3493-2019, 2019.
1033 Tang, G., Wang, Y., Li, X., Ji, D., Hsu, S., and Gao, X.: Spatial-temporal variations in surface ozone

https://doi.org/10.5194/acp-2019-788
Preprint. Discussion started: 16 December 2019


Atmospheric Chemistry and Physics Discussions

in Northern China as observed during 2009–2010 and possible implications for future air quality control strategies, Atmos Chem Phys, 12, 2757-2776, doi:10.5194/acp-12-2757-2012, 2012.

Tang, M., Huang, X., Lu, K., Ge, M., Li, Y., Cheng, P., Zhu, T., Ding, A., Zhang, Y., Gligorovski, S., Song, W., Ding, X., Bi, X., and Wang, X.: Heterogeneous reactions of mineral dust aerosol: implications for tropospheric oxidation capacity, Atmos Chem Phys, 17, 11727-11777, doi:10.5194/acp-17-11727-2017, 2017.

Tham, Y. J., Wang, Z., Li, Q., Wang, W., Wang, X., Lu, K., Ma, N., Yan, C., Kecorius, S., Wiedensohler, A., Zhang, Y., and Wang, T.: Heterogeneous N2O5 uptake coefficient and production yield of ClNO2 in polluted northern China: roles of aerosol water content and chemical composition, Atmos Chem Phys, 18, 13155-13171, doi:10.5194/acp-18-13155-2018, 2018.

Vereecken, L., and Francisco, J. S.: Theoretical studies of atmospheric reaction mechanisms in the troposphere, Chem Soc Rev, 41, 6259-6293, doi:10.1039/c2cs35070j, 2012.

Wang, M., Zeng, L., Lu, S., Shao, M., Liu, X., Yu, X., Chen, W., Yuan, B., Zhang, Q., Hu, M., and Zhang, Z.: Development and validation of a cryogen-free automatic gas chromatograph system (GC-MS/FID) for online measurements of volatile organic compounds, Anal. Methods, 6, 9424-9434, doi:10.1039/c4ay01855a, 2014a.

Wang, W., Li, X., Shao, M., Hu, M., Zeng, L., Wu, Y., and Tan, T.: The impact of aerosols on photolysis frequencies and ozone production in Beijing during the 4-year period 2012–2015, Atmos Chem Phys, 19, 9413-9429, doi:10.5194/acp-19-9413-2019, 2019a.

Wang, Y., Hu, B., Tang, G., Ji, D., Zhang, H., Bai, J., Wang, X., and Wang, Y.: Characteristics of ozone and its precursors in Northern China: A comparative study of three sites, Atmos Res, 132-133, 450-459, https://doi.org/10.1016/j.atmosres.2013.04.005, 2013.

Wang, Y., Wang, Y., Wang, L., Petäjä, T., Zha, Q., Gong, C., Li, S., Pan, Y., Hu, B., Xin, J., and Kulmala, M.: Increased inorganic aerosol fraction contributes to air pollution and haze in China, Atmos. Chem. Phys., 19, 5881-5888, doi:10.5194/acp-19-5881-2019, 2019b.

Wang, Y. H., Hu, B., Ji, D. S., Liu, Z. R., Tang, G. Q., Xin, J. Y., Zhang, H. X., Song, T., Wang, L. L., Gao, W. K., Wang, X. K., and Wang, Y. S.: Ozone weekend effects in the Beijing–Tianjin–Hebei metropolitan area, China, Atmos Chem Phys, 14, 2419-2429, doi:10.5194/acp-14-2419-2014, 2014b.

Warneke, C.: Comparison of daytime and nighttime oxidation of biogenic and anthropogenic VOCs

https://doi.org/10.5194/acp-2019-788
Preprint. Discussion started: 16 December 2019




1064 along the New England coast in summer during New England Air Quality Study 2002, Journal of
1065 Geophysical Research, 109, D10309, doi:10.1029/2003jd004424, 2004.
1066 Whalley, L. K., Stone, D., Bandy, B., Dunmore, R., Hamilton, J. F., Hopkins, J., Lee, J. D., Lewis,
1067 A. C., and Heard, D. E.: Atmospheric OH reactivity in central London: observations, model
1068 predictions and estimates of in situ ozone production, Atmos Chem Phys, 16, 2109-2122,
1069 doi:10.5194/acp-16-2109-2016, 2016.
1070 Williams, J., Keßel, S. U., Nölscher, A. C., Yang, Y., Lee, Y., Yáñez-Serrano, A. M., Wolff, S.,
1071 Kesselmeier, J., Klüpfel, T., Lelieveld, J., and Shao, M.: Opposite OH reactivity and ozone cycles
1072 in the Amazon rainforest and megacity Beijing: Subversion of biospheric oxidant control by
1073 anthropogenic emissions, Atmos Environ, 125, 112-118, doi:10.1016/j.atmosenv.2015.11.007, 2016.
1074 Wu, R., Li, J., Hao, Y., Li, Y., Zeng, L., and Xie, S.: Evolution process and sources of ambient
1075 volatile organic compounds during a severe haze event in Beijing, China, Sci Total Environ, 560-
1076 561, 62-72, doi:10.1016/j.scitotenv.2016.04.030, 2016.
1077 Xin, J. Y., Wang, Y. S., Tang, G. Q., Wang, L. L., Sun, Y., Wang, Y. H., Hu, B., Song, T., Ji, D. S.,
1078 and Wang, W. F.: Variability and reduction of atmospheric pollutants in Beijing and its surrounding
1079 area during the Beijing 2008 Olympic Games, Chinese Sci Bull, 55, 1937-1944, doi:
1080 10.1007/s00376-012-1227-4, 2010.
1081 Xue, L., Gu, R., Wang, T., Wang, X., Saunders, S., Blake, D., Louie, P. K. K., Luk, C. W. Y., Simpson,
1082 I., Xu, Z., Wang, Z., Gao, Y., Lee, S., Mellouki, A., and Wang, W.: Oxidative capacity and radical
1083 chemistry in the polluted atmosphere of Hong Kong and Pearl River Delta region: analysis of a
1084 severe photochemical smog episode, Atmos Chem Phys, 16, 9891-9903, doi:10.5194/acp-16-9891-
1085 2016, 2016.
1086 Yang, Y., Shao, M., Wang, X., Nölscher, A. C., Kessel, S., Guenther, A., and Williams, J.: Towards
1087 a quantitative understanding of total OH reactivity: A review, Atmos Environ, 134, 147-161,
1088 doi:10.1016/j.atmosenv.2016.03.010, 2016.
1089 Yang, Y., Shao, M., Keßel, S., Li, Y., Lu, K., Lu, S., Williams, J., Zhang, Y., Zeng, L., Nölscher, A.
1090 C., Wu, Y., Wang, X., and Zheng, J.: How the OH reactivity affects the ozone production efficiency:
1091 case studies in Beijing and Heshan, China, Atmos Chem Phys, 17, 7127-7142, doi:10.5194/acp-17-
1092 7127-2017, 2017.
1093 Yang, Y., Ji, D., Sun, J., Wang, Y., Yao, D., Zhao, S., Yu, X., Zeng, L., Zhang, R., Zhang, H., Wang,

https://doi.org/10.5194/acp-2019-788
Preprint. Discussion started: 16 December 2019


Atmospheric Chemistry and Physics Discussions

Y., and Wang, Y.: Ambient volatile organic compounds in a suburban site between Beijing and Tianjin: Concentration levels, source apportionment and health risk assessment, Sci Total Environ, 133889, https://doi.org/10.1016/j.scitotenv.2019.133889, 2019.

Ye, Y., Galbally, I., and Weeks, I.: Emission of 1,3-butadiene from petrol-driven motor vehicles, Atmos Environ, 31, 1157-1165, doi:10.1016/S1352-2310(96)00308-1, 1997.

Yoshino, A., Sadanaga, Y., Watanabe, K., Kato, S., Miyakawa, Y., Matsumoto, J., and Kajii, Y.: Measurement of total OH reactivity by laser-induced pump and probe technique—comprehensive observations in the urban atmosphere of Tokyo, Atmos Environ, 40, 7869-7881, doi:10.1016/j.atmosenv.2006.07.023, 2006.

Yuan, B., Shao, M., de Gouw, J., Parrish, D. D., Lu, S., Wang, M., Zeng, L., Zhang, Q., Song, Y., Zhang, J., and Hu, M.: Volatile organic compounds (VOCs) in urban air: How chemistry affects the interpretation of positive matrix factorization (PMF) analysis, Journal of Geophysical Research: Atmospheres, 117, 24302, doi:10.1029/2012jd018236, 2012.

Yuan, B., Hu, W. W., Shao, M., Wang, M., Chen, W. T., Lu, S. H., Zeng, L. M., and Hu, M.: VOC emissions, evolutions and contributions to SOA formation at a receptor site in eastern China, Atmos Chem Phys, 13, 8815-8832, doi:10.5194/acp-13-8815-2013, 2013.

Yuan, Z. B., Lau, A. K. H., Shao, M., Louie, P. K. K., Liu, S. C., and Zhu, T.: Source analysis of volatile organic compounds by positive matrix factorization in urban and rural environments in Beijing, J Geophys Res-Atmos, 114, doi:10.1029/2008JD011190, 2009.

Zannoni, N., Gros, V., Lanza, M., Sarda, R., Bonsang, B., Kalogridis, C., Preunkert, S., Legrand, M., Jambert, C., Boissard, C., and Lathiere, J.: OH reactivity and concentrations of biogenic volatile organic compounds in a Mediterranean forest of downy oak trees, Atmos Chem Phys, 16, 1619-1636, doi:10.5194/acp-16-1619-2016, 2016.

Zannoni, N., Gros, V., Sarda Esteve, R., Kalogridis, C., Michoud, V., Dusanter, S., Sauvage, S., Locoge, N., Colomb, A., and Bonsang, B.: Summertime OH reactivity from a receptor coastal site in the Mediterranean Basin, Atmos Chem Phys, 17, 12645-12658, doi:10.5194/acp-17-12645-2017, 2017.

Zheng, H., Kong, S. F., Xing, X. L., Mao, Y., Hu, T. P., Ding, Y., Li, G., Liu, D. T., Li, S. L., and Qi, S. H.: Monitoring of volatile organic compounds (VOCs) from an oil and gas station in northwest China for 1 year, Atmos Chem Phys, 18, 4567-4595, doi:10.5194/acp-18-4567-2018, 2018.

https://doi.org/10.5194/acp-2019-788
Preprint. Discussion started: 16 December 2019


Atmospheric Chemistry and Physics Discussions

1124

1125 **Figure captions**

1126

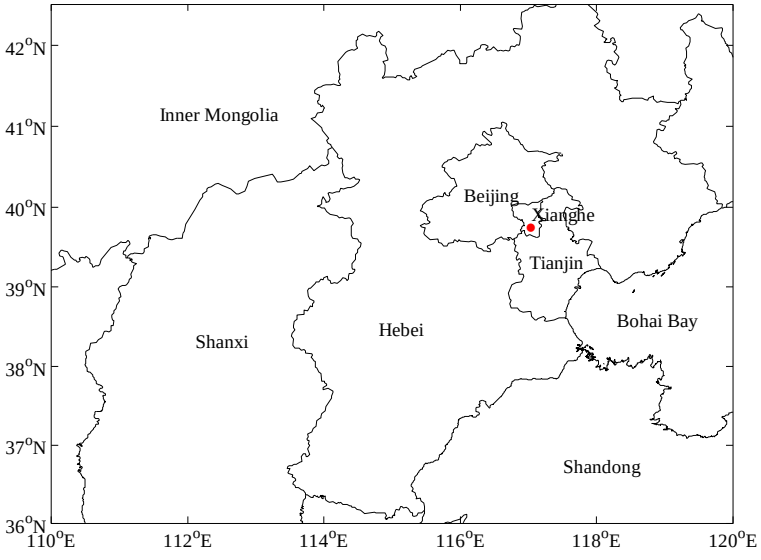


1127 Figure 1. The location of the sampling site, which is marked with a red dot. The blacklines are
1128 provincial boundary lines of each province. (The figure was produced by MATLAB 2017a).

1129

1130

1131

1132

1133

1134

1135

1136

1137

https://doi.org/10.5194/acp-2019-788
Preprint. Discussion started: 16 December 2019


Atmospheric Chemistry and Physics Discussions

1138

1139

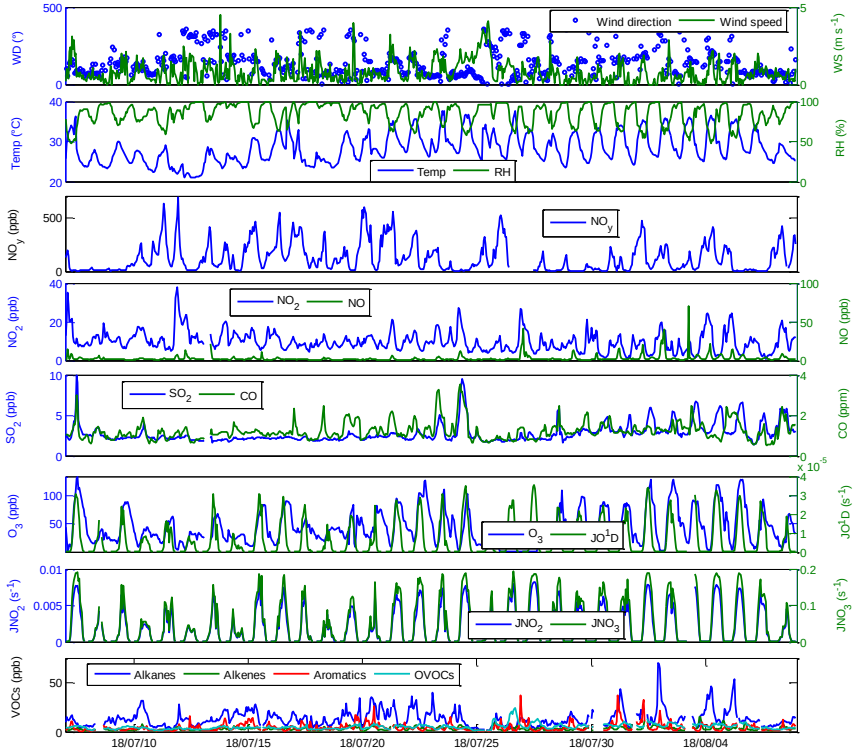


1140

1141 Figure 2. Time series of meteorology parameters, trace gases, photolysis rates of $JNO_2$ and $JNO_3$,

1142 and VOCs concentrations during the field campaign at Xianghe from 6 July to 6 August 2018.

1143

1144

1145

1146

1147

1148

https://doi.org/10.5194/acp-2019-788
Preprint. Discussion started: 16 December 2019


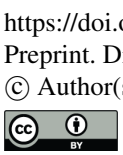

Atmospheric Chemistry and Physics Discussions

1149

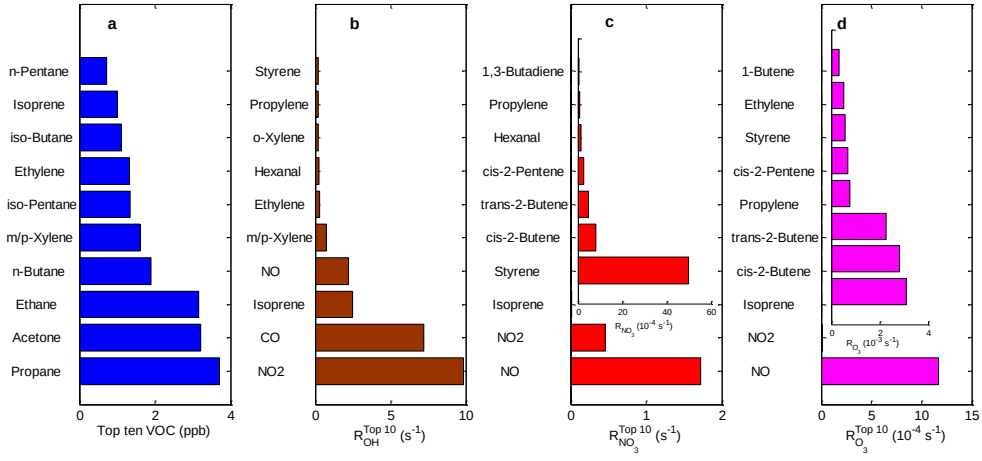


1150

1151 Figure 3. The top ten abundant VOC species (a), reactivity of OH ($R_{OH}^{\text{calculated}}$) (b), reactivity of $NO_3$

1152 ($R_{NO_3}^{\text{calculated}}$) (c) and reactivity of $O_3$ ($R_{O_3}^{\text{calculated}}$) (d) during the field campaign at Xianghe from

1153 6 July to 6 August 2018.

1154

1155

1156

1157

1158

1159

1160

1161

1162

https://doi.org/10.5194/acp-2019-788
Preprint. Discussion started: 16 December 2019


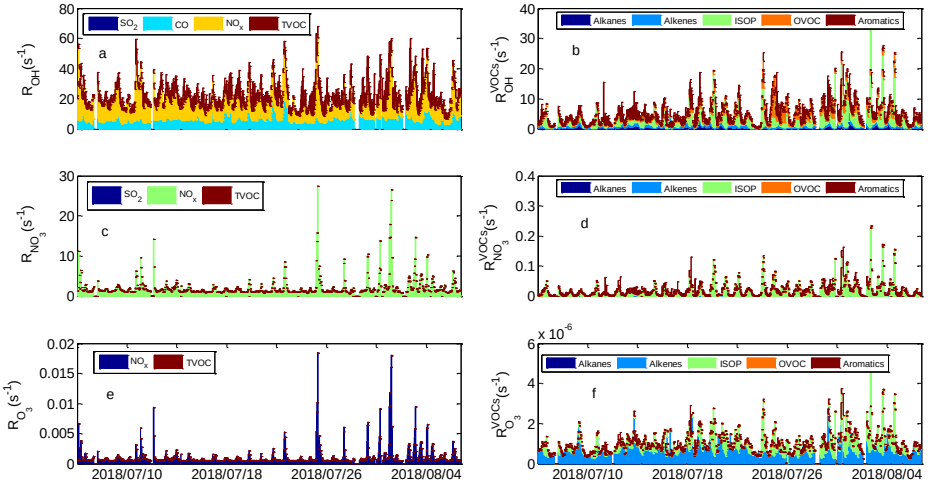


Figure 4. The time series of $R_{OH}^{\text{calculated}}$, $R_{NO_3}^{\text{calculated}}$ and $R_{O_3}^{\text{calculated}}$ during the field campaign at Xianghe from 6 July to 6 August 2018.

https://doi.org/10.5194/acp-2019-788
Preprint. Discussion started: 16 December 2019


Atmospheric Chemistry and Physics Discussions

1175

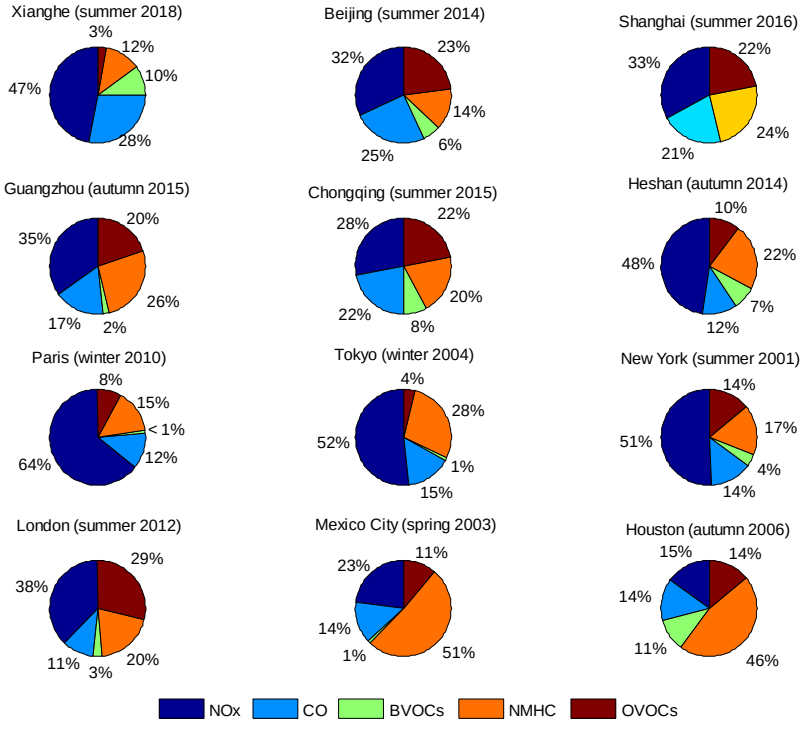


1176 Figure 5. Contributions of different atmospheric compounds to $R_{OH}$ at Xianghe (summer 2018,
1177 this study), Beijing (summer 2014, Tan et al., 2019), Shanghai (summer 2016, Tan et al., 2019),
1178 Guangzhou (autumn 2015, Tan et al., 2019), Chongqing (summer 2015, Tan et al., 2019), Heshan
1179 (autumn 2014, Yang et al., 2017), Paris (winter 2010, Dolgorouky et al., 2012), Tokyo (winter 2004,
1180 Yoshino et al., 2006), New York (summer 2001, Mao et al., 2010), London (summer 2012, Whalley
1181 et al., 2016), Mexico City (spring 2003, Mao et al., 2010) and Houston (autumn 2006, Mao et al.,
1182 2010).

1183

1184

1185

1186

1187

https://doi.org/10.5194/acp-2019-788
Preprint. Discussion started: 16 December 2019


Atmospheric Chemistry and Physics Discussions

1188

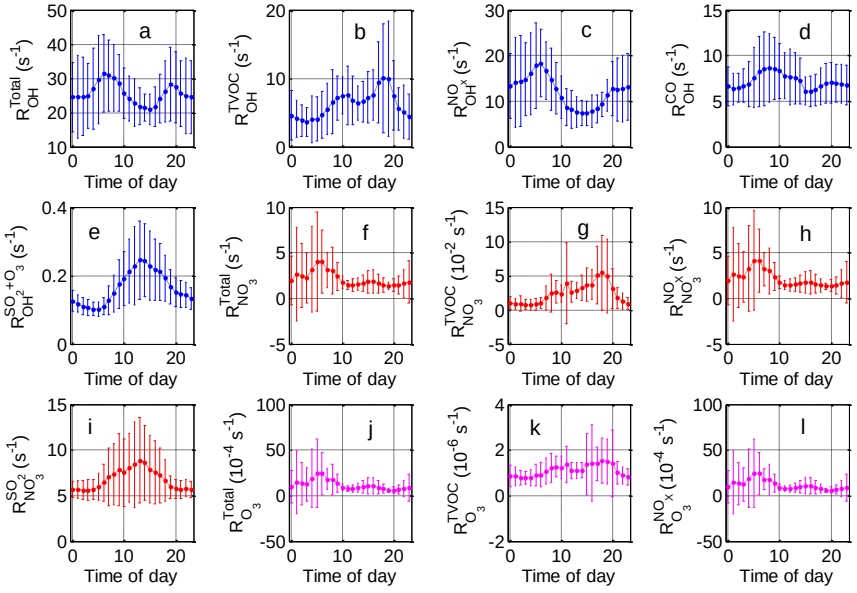


1189 Figure 6. Mean diurnal variations of $R_{OH}^{\text{calculated}}$, $R_{NO_3}^{\text{calculated}}$ and $R_{O_3}^{\text{calculated}}$ of trace gases during

1190 the field campaign at Xianghe from 6 July to 6 August 2018.

1191

1192

1193

1194

1195

1196

1197

1198

1199

1200

https://doi.org/10.5194/acp-2019-788
Preprint. Discussion started: 16 December 2019


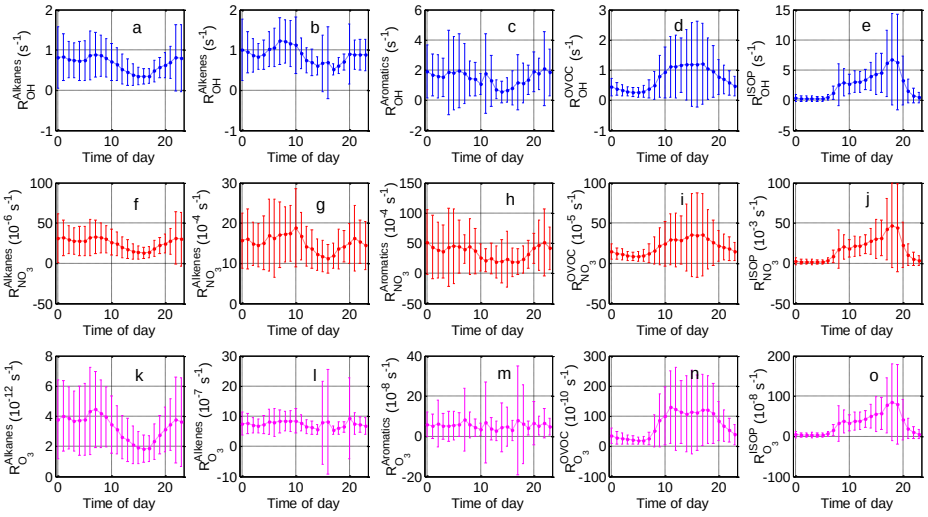


Figure 7. Mean diurnal variations of $R_{OH}^{\text{calculated}}$, $R_{NO_3}^{\text{calculated}}$ and $R_{O_3}^{\text{calculated}}$ of VOC groups during the field campaign at Xianghe from 6 July to 6 August 2018.

https://doi.org/10.5194/acp-2019-788
Preprint. Discussion started: 16 December 2019


Atmospheric Chemistry and Physics Discussions

1214

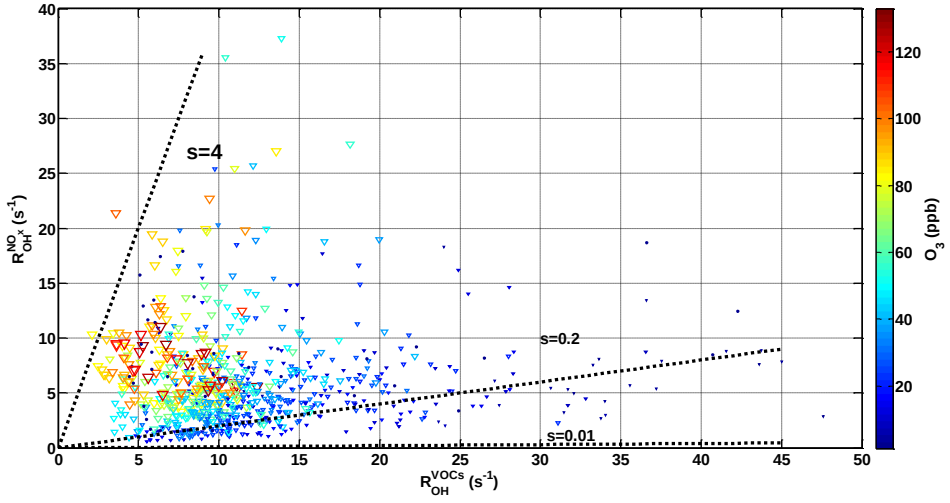


1215 Figure 8. $O_3$ production regimes at Xianghe station. The dot lines are the borders of the three regimes
1216 of $O_3$ formation. "s" denotes the relative reactivity of OH towards $NO_x$ and VOCs. For s > 0.2: VOC
1217 limitation, for s < 0.01: $NO_x$ limitation of the $O_3$ formation.

1218

1219

1220

1221

1222

1223

1224

1225

1226

https://doi.org/10.5194/acp-2019-788
Preprint. Discussion started: 16 December 2019


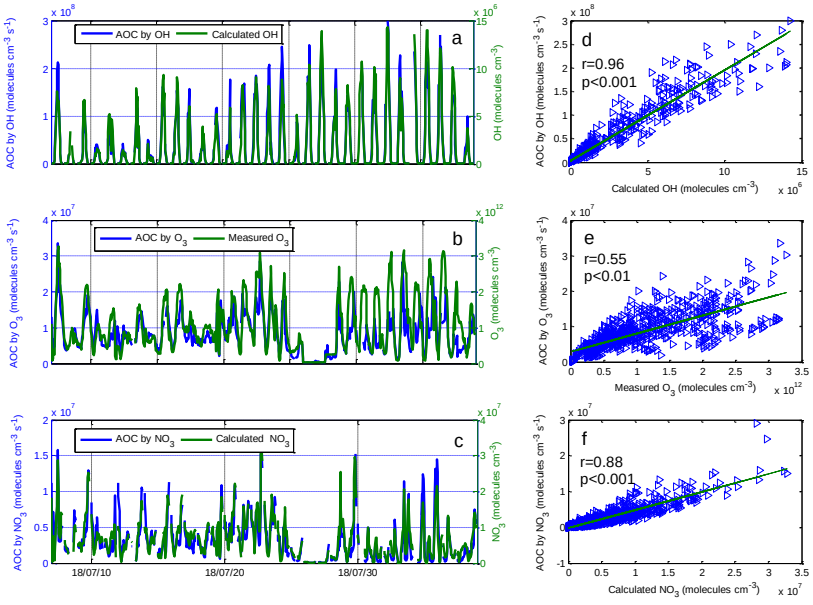


Figure 9. Comparisons of calculated AOC by OH (a), $O_3$ (b) and $NO_3$ (c), and corresponding oxidation concentrations. The left column shows the time series and the right column shows scatterplots of calculated AOC and corresponding oxidation concentrations. Note: r and p are the correlation coefficient and the significance level, respectively.

https://doi.org/10.5194/acp-2019-788
Preprint. Discussion started: 16 December 2019


Atmospheric Chemistry and Physics Discussions

1240

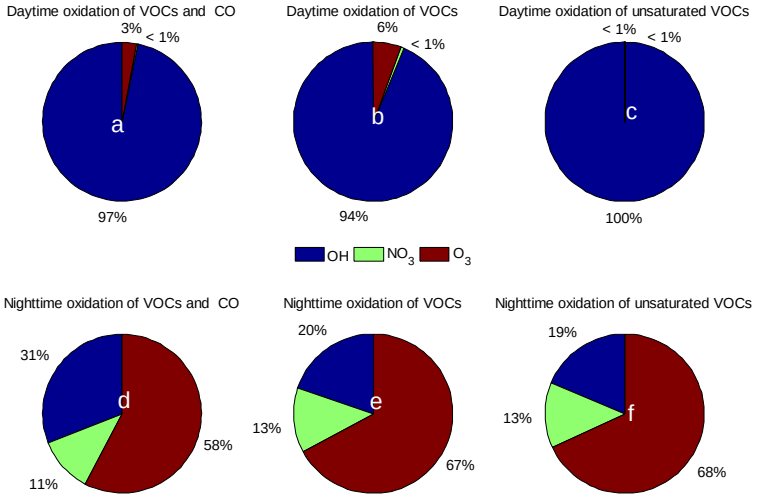


1241 Figure 10. Comparison of the relative contributions of OH, $NO_3$ and $O_3$ to the daytime and nighttime
1242 integral of the oxidation rates. Data are calculated for the oxidation of (a,d) VOCs and CO, (b,e)
1243 VOCs only, and (c,f) unsaturated VOCs only.

1244

1245

1246

1247

1248

1249

1250

1251

https://doi.org/10.5194/acp-2019-788
Preprint. Discussion started: 16 December 2019


Atmospheric Chemistry and Physics Discussions

1252

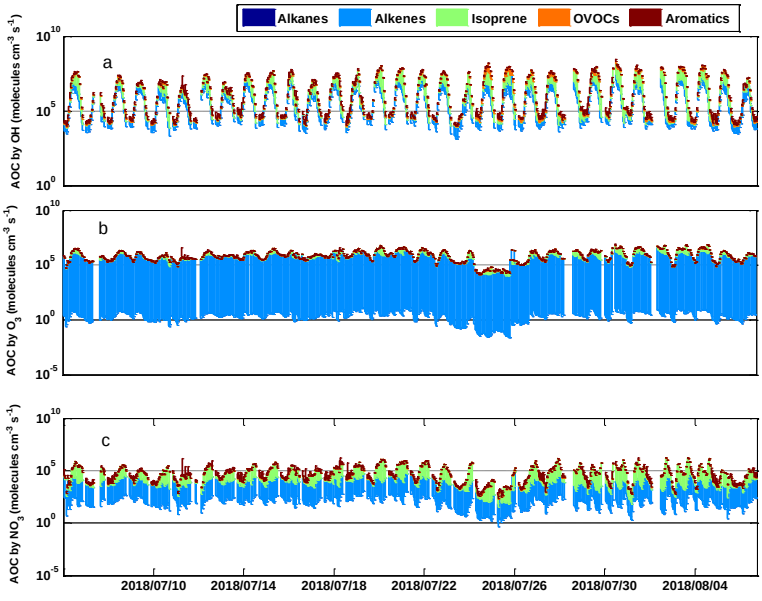


1253 Figure 11. The time series of VOC loss rates due to the reactions with OH radical, $O_3$ and $NO_3$

1254 radical.

1255

1256

1257

1258

1259

1260

1261

1262

1263

1264

https://doi.org/10.5194/acp-2019-788
Preprint. Discussion started: 16 December 2019


Atmospheric Chemistry and Physics Discussions

1265

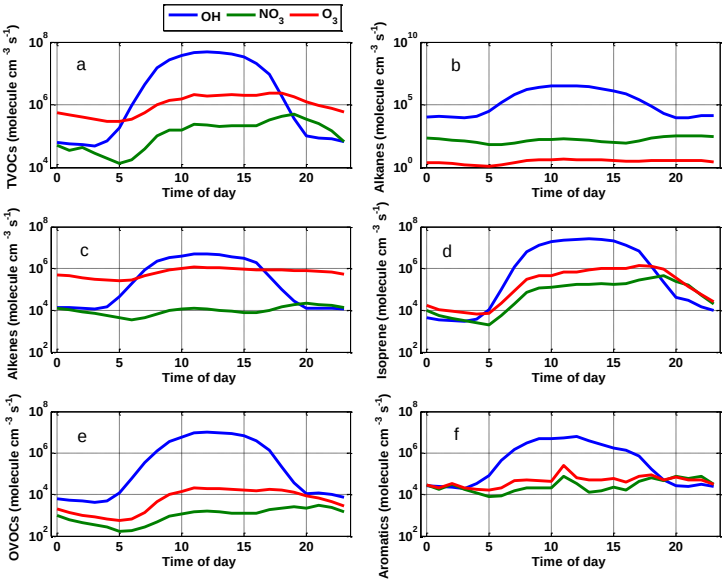


1266 Figure 12. Diurnal variations of VOC loss rates due to the reactions with OH radical (blue lines),

1267 $NO_3$ radical (green lines) and $O_3$ (red lines).

1268

1269

1270

1271

1272

1273

1274

1275

https://doi.org/10.5194/acp-2019-788
Preprint. Discussion started: 16 December 2019


Atmospheric Chemistry and Physics Discussions

1276

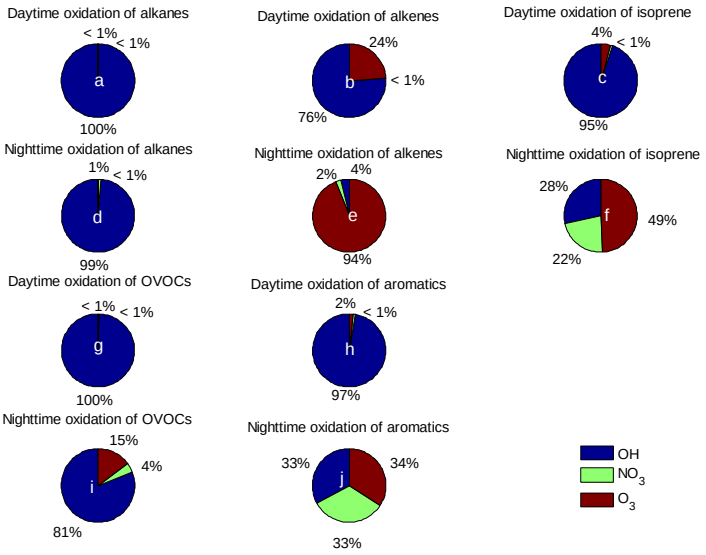


1277 Figure 13. Comparison of the relative contributions of OH, $NO_3$ and $O_3$ to the daytime and nighttime
1278 integral of the oxidation rates. Data are calculated for the oxidation of (a,d) alkanes, (b,e) alkenes,
1279 (c,f) isoprene, (g,i) OVOCs and (h,j) aromatics.

1280

1281

1282

1283

1284

1285

1286

1287

1288

1289

https://doi.org/10.5194/acp-2019-788
Preprint. Discussion started: 16 December 2019


Atmospheric Chemistry and Physics Discussions

1290 **Table captions**

1291 Table 1. The top 10 VOCs species in terms of concentration (first column), $R_{OH}$ (second column),
1292 $R_{NO_3}$ (third column) and $R_{O_3}$ (fourth column) and their corresponding contributions to
1293 concentration, $R_{OH}$, $R_{NO_3}$ and $R_{O_3}$ (%).

1294

| First column | | | | | Second column | | | | |
|---|---|---|---|---|---|---|---|---|---|
| **Species** | **Concentration** | $R_{OH}$ | $R_{NO_3}$ | $R_{O_3}$ | **Species** | **Concentration** | $R_{OH}$ | $R_{NO_3}$ | $R_{O_3}$ |
| Propane | **14.6** | 2.7 | 0.1 | 0.0 | m/p-Xylene | 6.4 | **20.1** | 0.1 | 0.0 |
| Acetone | **12.7** | 0.4 | 0.0 | 0.1 | Ethylene | 5.3 | **7.3** | 0.1 | 6.3 |
| Ethane | **12.5** | 0.5 | 0.0 | 0.0 | Hexanal | 1.3 | **6.6** | 1.9 | 0.0 |
| n-Butane | **7.5** | 3.0 | 0.0 | 0.0 | o-Xylene | 2.6 | **5.8** | 0.1 | 0.0 |
| m/p-Xylene | **6.4** | 20.1 | 0.1 | 0.0 | Propylene | 1.2 | **5.4** | 1.0 | 9.3 |
| iso-Pentane | **5.3** | 3.2 | 0.1 | 0.0 | Styrene | 0.5 | **5.2** | 72.0 | 6.8 |
| Ethylene | **5.3** | 7.3 | 0.1 | 6.3 | Methacrolein | 0.8 | **3.9** | 0.2 | 0.7 |
| iso-Butane | **4.4** | 1.6 | 0.0 | 0.0 | cis-2-Butene | 0.4 | **3.9** | 11.5 | 34.0 |
| n-Pentane | **2.8** | 1.8 | 0.0 | 0.0 | MethylVinylKetone | 1.1 | **3.7** | 0.1 | 0.0 |
| Toluene | **2.6** | 2.5 | 0.0 | 0.0 | iso-Pentane | 5.3 | **3.2** | 0.1 | 0.0 |
| **Third column** | | | | | **Forth column** | | | | |
| **Species** | **Concentration** | $R_{OH}$ | $R_{NO_3}$ | $R_{O_3}$ | **Species** | **Concentration** | $R_{OH}$ | $R_{NO_3}$ | $R_{O_3}$ |
| Styrene | 0.5 | 5.2 | **72.0** | 6.8 | cis-2-Butene | 0.4 | 3.9 | 11.5 | **34.0** |
| cis-2-Butene | 0.4 | 3.9 | **11.5** | 34.0 | trans-2-Butene | 0.2 | 1.8 | 6.7 | **27.3** |
| trans-2-Butene | 0.2 | 1.8 | **6.7** | 27.3 | Propylene | 1.2 | 5.4 | 1.0 | **9.3** |
| cis-2-Pentene | 0.1 | 0.9 | **2.8** | 8.1 | cis-2-Pentene | 0.1 | 0.9 | 2.8 | **8.1** |
| Hexanal | 1.3 | 6.6 | **1.9** | 0.0 | Styrene | 0.5 | 5.2 | 72.0 | **6.8** |
| Propylene | 1.2 | 5.4 | **1.0** | 9.3 | Ethylene | 5.3 | 7.3 | 0.1 | **6.3** |
| 1,3-Butadiene | 0.1 | 0.9 | **0.7** | 0.4 | 1-Butene | 0.5 | 2.7 | 0.6 | **3.7** |
| 1-Butene | 0.5 | 2.7 | **0.6** | 3.7 | trans-2-Pentene | 0.0 | 0.2 | 0.5 | **1.8** |
| trans-2-Pentene | 0.0 | 0.2 | **0.5** | 1.8 | 1-Pentene | 0.1 | 0.6 | 0.2 | **0.9** |
| Pentanal | 0.2 | 1.1 | **0.3** | 0.0 | Methacrolein | 0.8 | 3.9 | 0.2 | **0.7** |

1295